X-713-66-79

NASA TM X-55505

THE SPECTRAL DISTRIBUTION AND UNIFORMITY OF THE CARBON ARC

MARCH 1966

NASA — GODDARD SPACE FLIGHT CENTER

GREENBELT, MARYLAND

X-713-66-79

THE SPECTRAL DISTRIBUTION AND UNIFORMITY OF THE CARBON ARC

by

Steve Alexander*
Radiometry Group
Thermal Systems Branch
Spacecraft Technology Division

March 1966

Goddard Space Flight Center
Greenbelt, Maryland

*National Science Foundation trainee at G.S.F.C.

THE SPECTRAL DISTRIBUTION AND UNIFORMITY OF THE CARBON ARC

by

Steve Alexander
Radiometry Group
Thermal Systems Branch
Spacecraft Technology Division

30328

ABSTRACT

The uniformity and spectral irradiance of a Genarco ME4CWM carbon arc have been determined. The uniformity using a one element lens system was ±14% over a 12 inch target area. The spectral irradiance of the bare arc is a fairly good match to the air mass zero solar irradiance. The arc has an excess of energy between 380 nm and 400 nm and from 1000 nm to 2600 nm and a deficiency of energy between 400 nm and 800 nm.

~~Goth~~ author

CONTENTS

THE SPECTRAL DISTRIBUTION AND UNIFORMITY OF THE CARBON ARC

INTRODUCTION

The carbon arc is thought by many in the field of solar simulation to be one of the better matches to the solar spectrum. It was the purpose of this experiment to obtain useful, accurate, data on the spectral distribution, uniformity, and temporal stability of the arc. Also included is a section on operation techniques and difficulties encountered.

Due to somewhat cramped quarters and a shortage of time, however, the variety and range of measurements were severely limited. It was hoped that data could be obtained on the spectral distribution in several planes, uniformity in several planes, and microbrightness contours of the arc. Distribution measurements were limited to one plane as were the uniformity scans. The microbrightness contours were not attempted.

INSTRUMENTATION

Three primary instruments and their various support apparatus were used to make the spectral irradiance measurements. They were the carbon arc, a Leiss double prism monochromator, and a data logging system manufactured by Control Equipment Corp., Neadham Heights, Mass. The uniformity measurements were taken with an unique instrument of special design. Figure 1 is a functional block diagram of the instrumentation.

The Genarco, Inc. Solar Radiation Simulator is comprised of a Genarco Metro-Lite Model #ME4CWM high intensity carbon arc lamp, an optically ground quartz lens to produce the required collimated beam of radiation, and a rectifier to supply the arc with the proper current. Figure 2 is a diagram of the arc.

The rectifier unit operates on 220 volts a.c., 3 phase, 60 amperes on each phase. Its d.c. output on open circuit is 90 to 100 volts, required to strike the arc; at full load, voltage is 60 to 65 volts, and the current is 185 amperes. For this experiment, rectifier voltage output was kept relatively constant at 57 ± 0.5 volts while the current varied randomly from 205 to 235 amperes as a function of resistance along the positive carbon.

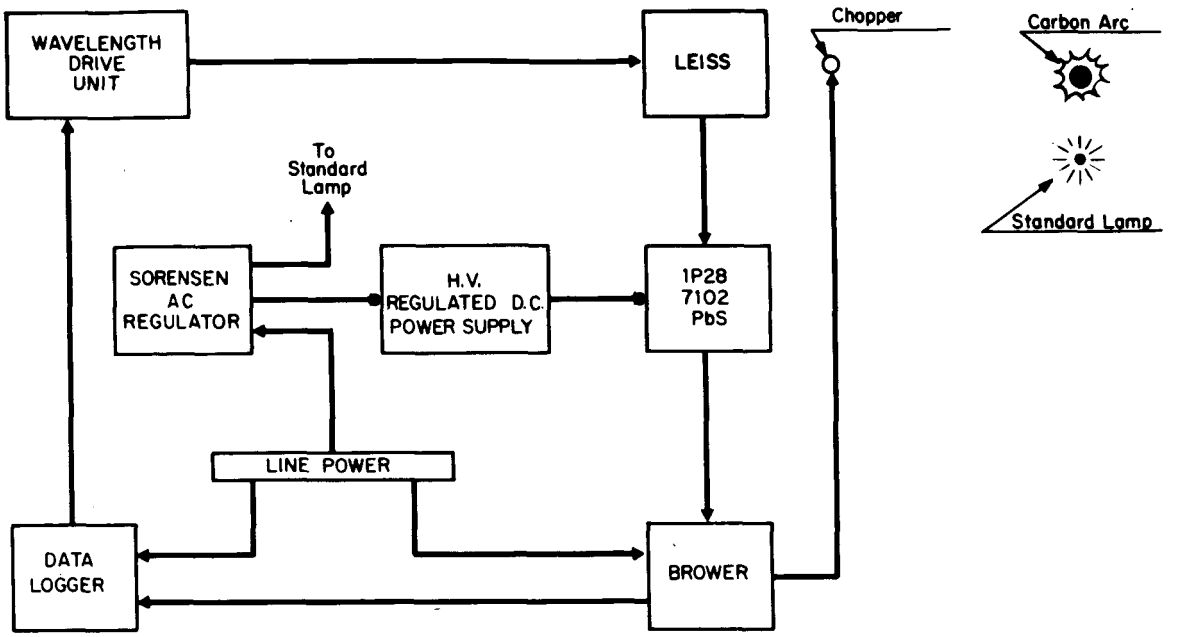

Figure 1–Spectral Distribution Instrumentation

The lamp itself is a tripod mounted encasement with nosepiece for the optical system and a magazine for handling the positive carbon assembly. The positive contacts, negative head and lamp body are water cooled requiring 5 gallons min^{-1} at 20 p.s.i.g. while the hot exhaust gases and ozone generated by the arc are removed by the blower assembly mounted on the lamp housing. Figure 3 is a photograph of the arc.

The carbons used are quality grade especially manufactured and machined by the Lorraine Carbon Co. of France. The positive carbon (Orlox 585-08) is 13.6 mm. in diameter and 22" long, is fed horizontally while the negative (Orlox 555-41) is 11.1 mm. in diameter and 48" long, is fed upwards at an angle of 53° to the positive. The arc gap is maintained relatively constant at 35/64" by two independently controlled feed motors (Figure 4).

The positive carbon feed control mechanism operates on a photo cell electron basis (Figure 5). The system is comprised of:

1. A small hole 'K' located in the lamp housing exactly opposite the positive carbon tip.
2. A miniature optical system consisting of a small lens and turning flat.
3. An imaging plate 'P' in which is a second hole 'H'.

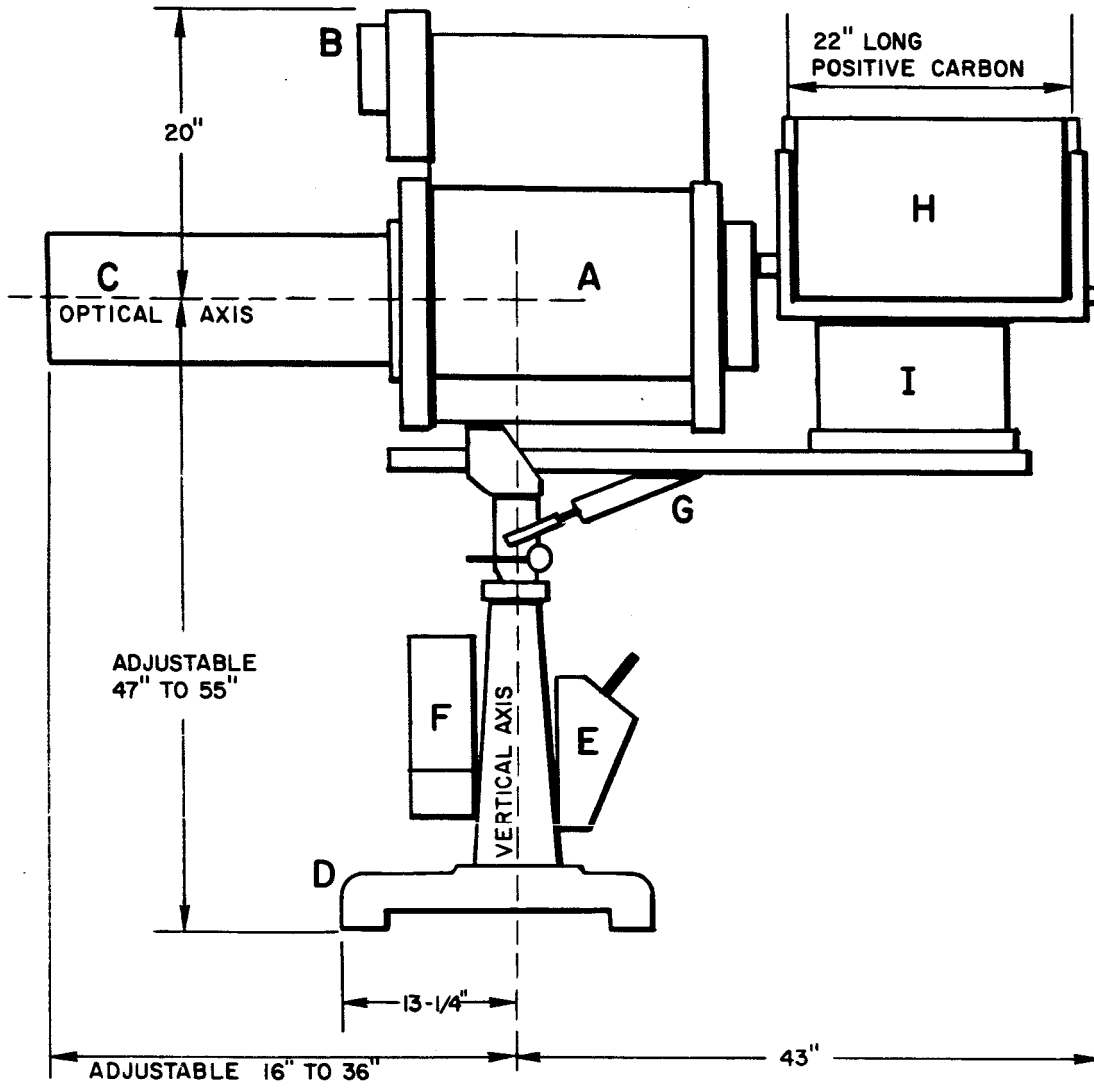

A. Lamphousing
B. Exhaust blower
C. Nosepiece containing Lens mounting
D. Tripod base
E. Knife switch
F. Electronic controls and pressure gauge housing
G. Optical axis' horizontal and vertical adjust mechanism
H. Positive carbon Magazine Rack
I. Magazine base housing rheostat plus positive and negative feed control indicators

Figure 2–Diagram of Genarco Model # ME4CWM

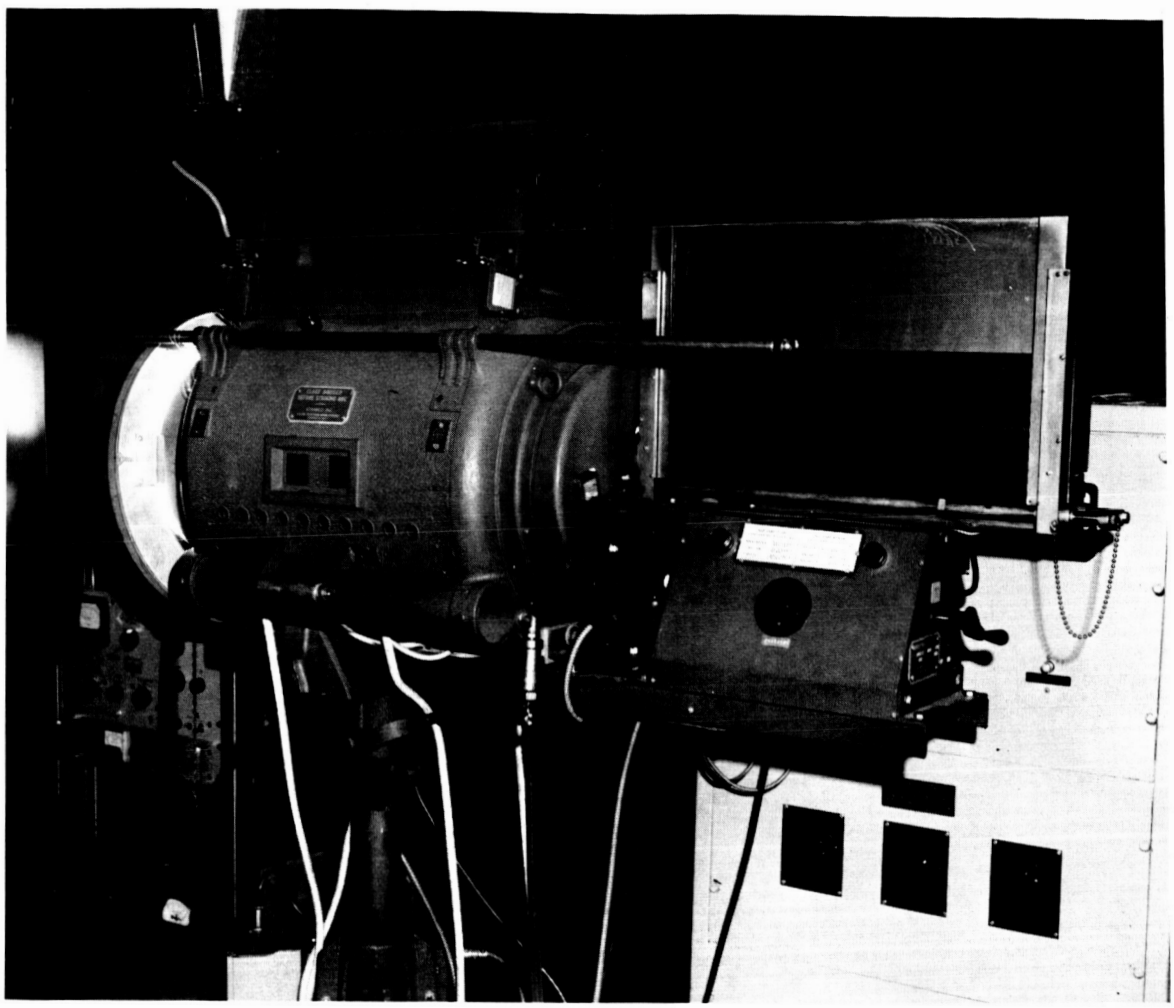

Figure 3–The Genarco Carbon Arc in Operation

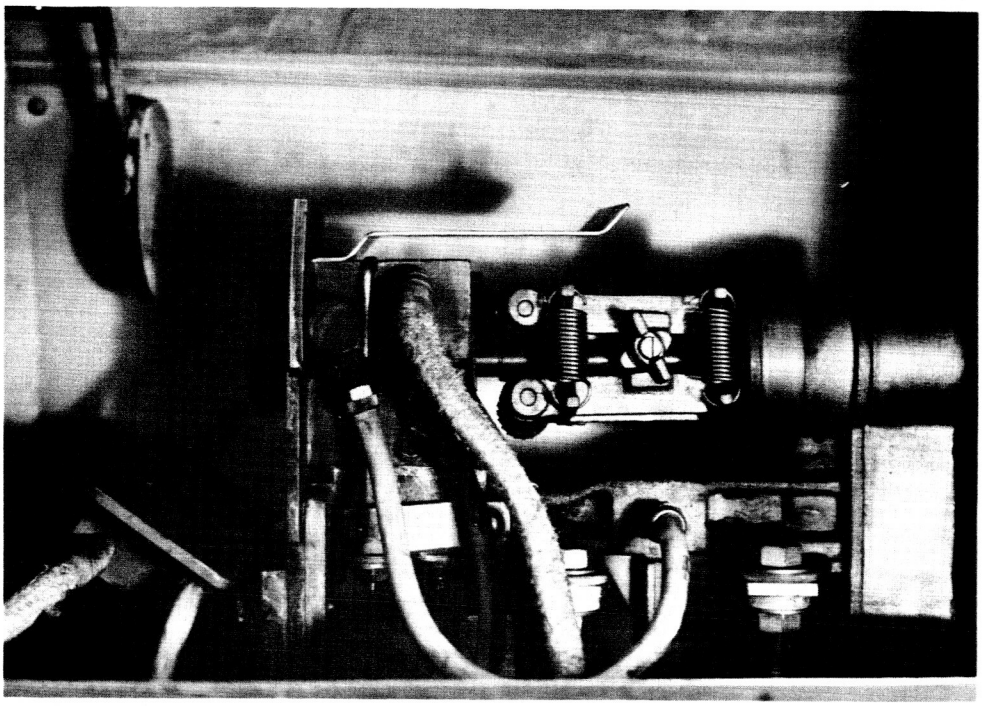

Figure 4–The Carbons, Contacts, and Feed Mechanism

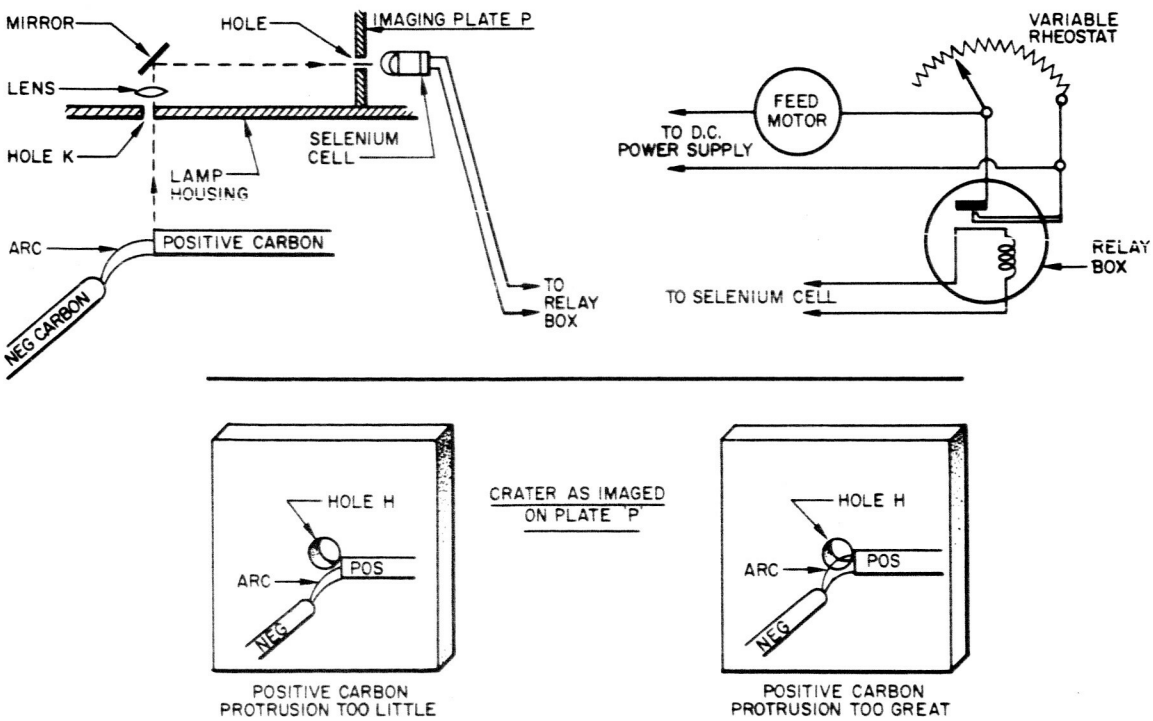

Figure 5–Positive Carbon Protrusion Monitoring and Control Device

4. A photo cell consisting of another lens and a selenium cell detector.

5. A relay switch, variable rheostat, and positive feed motor.

When the lamp is in operation, light from the burning positive tip is passed thru hole 'K' and focused on the turning flat by the lens. The image is deflected from the flat to the imaging plate 'P'. If the positive carbon protrusions is too little, the image forms on plate 'P' below hole 'H' and no light reaches the selenium cell. In this instance, the cells electrical resistance greatly increases causing a relay switch to close. This shorts the variable rheostat. Prior to shorting the rheostat, the positive feed motor operates at the speed determined by the rheostat setting. But, with the rheostat shorted, the motor receives full current and operates at maximum speed advancing the positive carbon very rapidly. When the positive carbon protrusion reaches a certain degree of advancement, or any greater degree, the arc image on plate 'P' is such that the selenium cell receives light. Its electrical resistance decreases; the relay switch reopens, and the motor returns to the "normal" operating speed as dictated by the rheostat setting.

The negative carbon feed control is similar in construction and operation to the positive control. There is one basic difference. Unlike the positive feed motor, the negative feed operates only when no light reaches the selenium cell. Automatic brakes stop the motor as soon as light reaches the cell. The negative feed mechanism does not operate continuously because negative carbon consumption is so little that it does not require constant advancement of the negative rod.

The positive carbons are supplied in a clip assembly, containing 24 carbons per clip, to facilitate reloading operations and to insure continuous arc operation over extended periods of time (Figure 6). When the male end of carbon P1 reaches

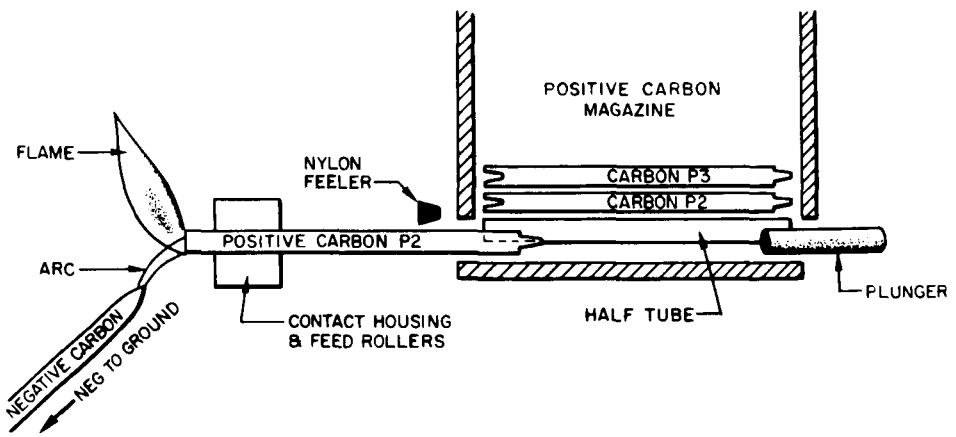

Figure 6–Automatic Reloading Mechanism

the nylon feeler, a magnetic switch is activated. The plunger is retracted; the half tube rotates, picking up carbon P2 and depositing it on the magazine base. The plunger is then released and drives P2 firmly into P1, forming a secure joint.

The optical system employed with the arc consists of an U.V. grade quartz lens and lens mounting. The lens is 12" in diameter and has a focal length of 21 inches. Also included is an iris mechanism for control of the beam diameter below 12" (Figure 7).

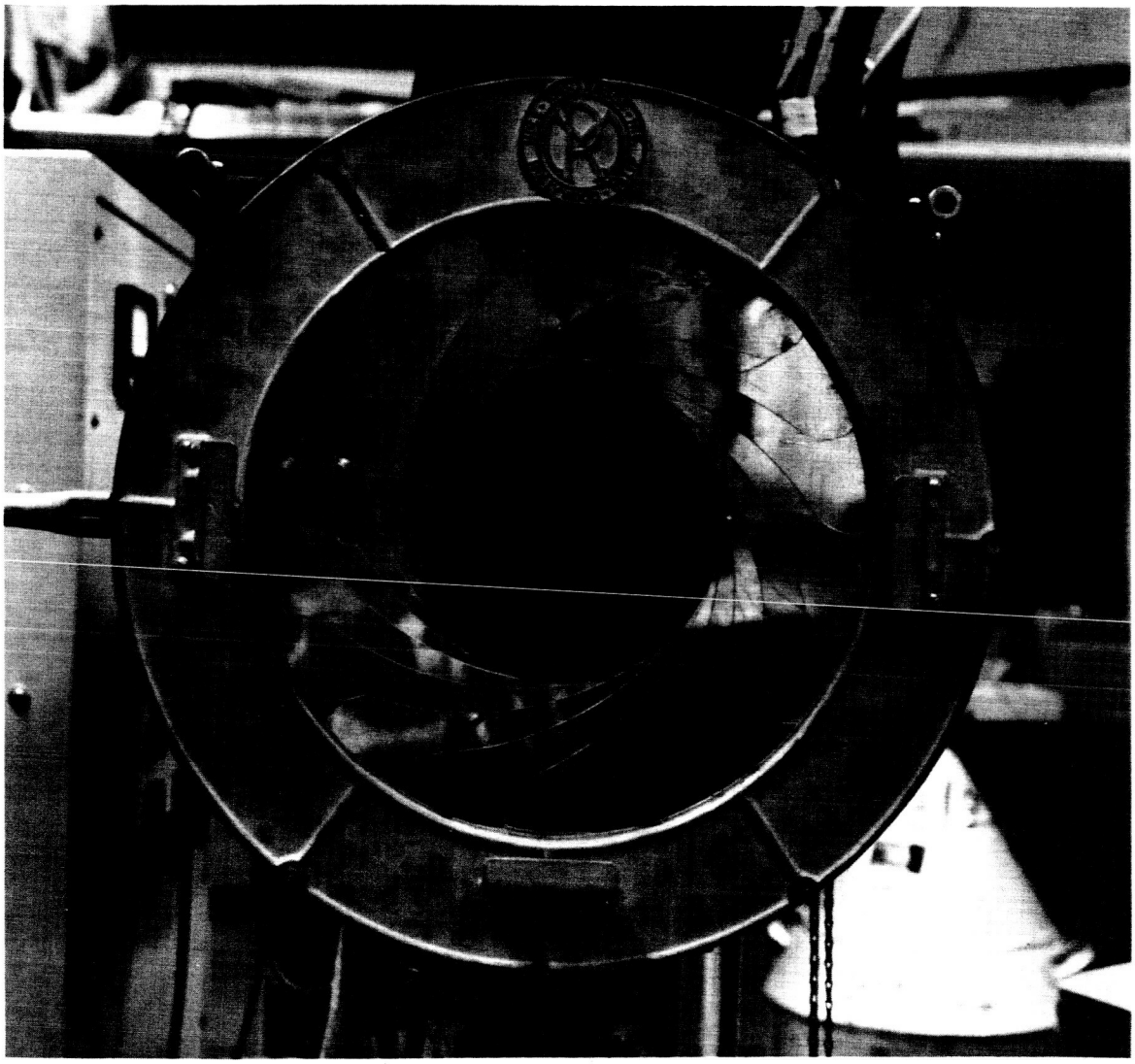

Figure 7–The Iris

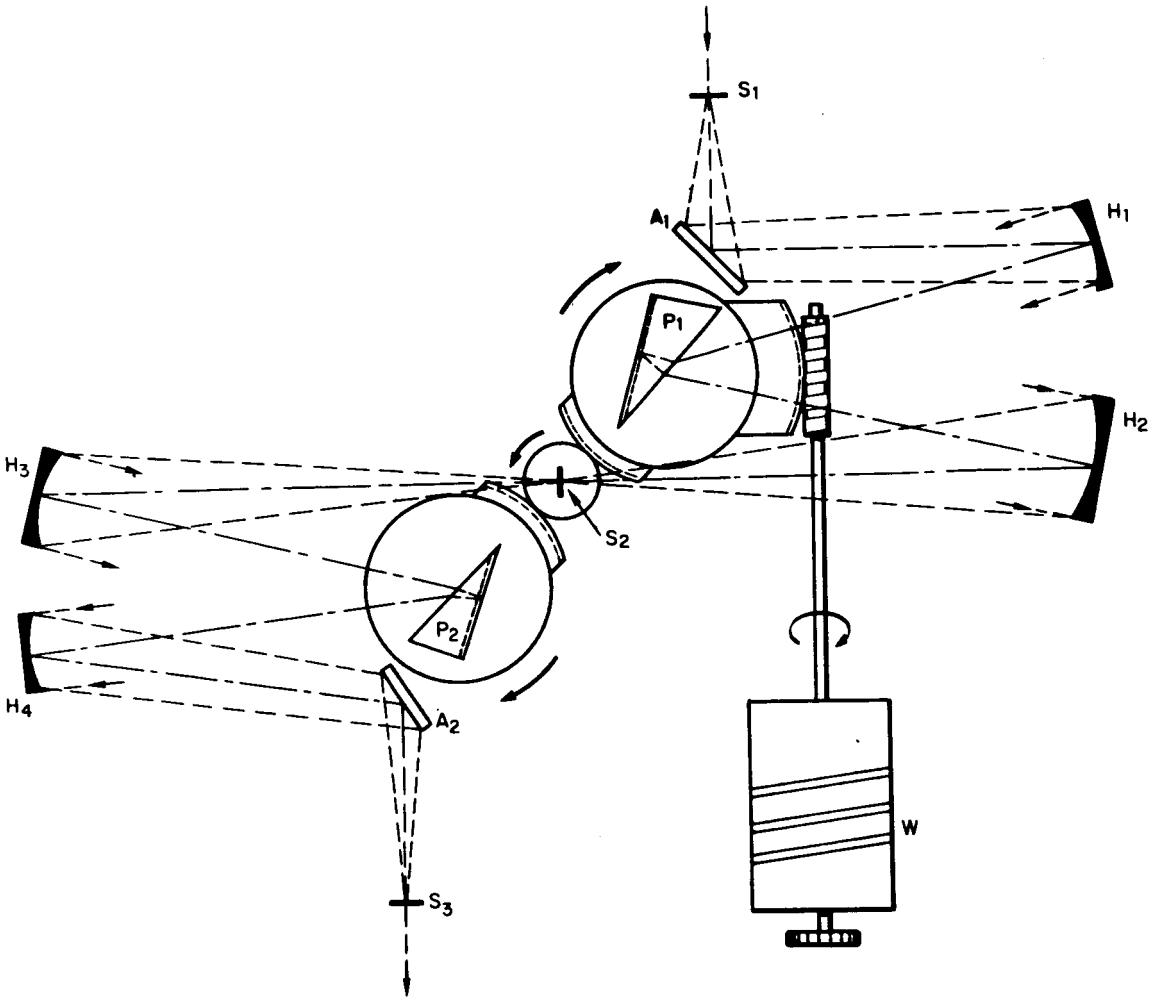

Figure 8–Optical Diagram of the Leiss Monochromator

The standard used for this experiment was a General Electric DXW/120v-1000 w., tungsten-quartz-iodine lamp. This lamp was calibrated by the National Bureau of Standards as a standard of spectral irradiance when operated at 8.3 amperes (125-130 volts).

A Leiss double prism monochromator, manufactured by Carl Leiss of West Germany, was used to disperse the light. An optical diagram is shown in Figure 8. Light from the source enters the monochromator at entrance slit 'S1' and is deflected to mirror 'H1' by the turning flat 'A1'. Flat A1 is so positioned that the ray of light forming the axis of the entering beam is deflected to the center of 'H1', a collimating mirror. Thus, light from 'A1' completely fills 'H1'. The parallel beam reflected from 'H1' is refracted by prism 'P1.' 'P1' has a mirror coating on its rear surface and reflects the spectrally dispersed

light to the concave mirror 'H2' from which it is focused on the plane of exit slit 'S2'. The divergent beam leaving 'S2' is recollimated by the second collimating mirror 'H3' and refracted by the second prism 'P2' so that, after reflection from the focusing mirror 'H4' and flat 'A2', any stray light which might have been in the beam at 'S2' is now thoroughly dispersed. Twice purified light of exceptional spectral clarity emerges from exit slit 'S3' to illuminate the detector face.

Prism 'P1' is securely connected to 'P2' to ensure that each is in spectral harmony with the other at all times. By rotating the wavelength drum 'W', one can flash across exit slit 'S3' the entire spectrum from 0.20 to 40.0 microns—depending upon the prism material used. The drum circumference is calibrated in 100 divisions and positions of 0.25 divisions can easily be estimated. One revolution of the drum represents a shift of prism position by 1°. Each prism position can be accurately reproduced to within ±10 seconds.

Each of the slits has a useable height of 10 mm., though the entrance slit 'S1' can be reduced to 1 mm. by use of a built in diaphragm. Slit widths are independently adjustable within a range from 0.01 mm. to 1.0 mm. Settings with an accuracy of 0.0025 mm. can easily be estimated with the unaided eye.

The two spherical concave mirrors, 'H1' and 'H4', have a useable surface of 55 × 57 mm. and a focal length of 300 mm. Each is coated with evaporated aluminum and has a reflectivity of approximately 90%.

The prisms are each 50 mm. high and have a hypotenuse of 75 mm. Their refracting angle varies from 30° to 35° depending upon the material used.

When spectral radiance measurements are made it is necessary to focus an image of the source on the plane of the entrance slit. However, for measurements of spectral irradiance, it is desirable to focus the source a few inches in front of the slit and allow the divergent beam to enter the monochromator. It would be even more desirable to irradiate the monochromator entrance slit with a portion of an entirely unfocused beam. Assuming that the source spectral characteristics are uniform through out the beam volume, the choice of any portion of the beam would not affect the measurements and would provide a true indication of the source spectral irradiance.

Great care must be exercised in making such measurements else significant error is introduced. Since detector responsivity is not uniform over the entire detecting surface, it is mandatory that the same area of the detector be used through out the experiment.

Illumination of the detector depends entirely upon the manner in which the light traverses the optical path of the monochromator. This, in turn, is dependent upon the illumination of the entrance slit. Thus, it is seen, the manner in which light arrives at the entrance slit is critical to the success of the experiment. The slit must be consistently illuminated in exactly the same manner by both test and standard lamps.

To accomplish this measurement with an unfocused beam is very nearly impossible without the aid of an external system of some design. Such a system was designed by and fabricated for the Radiometry Group in the form of an integrating sphere. It consists chiefly of an aluminum block, hollowed and machined to the form required (Figure 9), painted with optical flat black on the exterior and securely mounted on the Leiss in front of the entrance slit. It is so designed as to easily permit rotation. The interior is a perfect sphere measuring 4" in diameter and coated with MgO. The port on the flat of part 2 is that through which light enters the sphere. It measures 1" in external diameter and 1-7/16" in internal diameter. The slides slope at an angle of 30° to the vertical plane of the flat to ensure razor edges at the entrance and, hence, a better defined beam. At the rear surface of part 3 is a slit, 1/8" wide and 1/2" long, centered along the horizontal and parallel to the vertical axis. This is the exit slit.

The entrance port was placed off the center axis to insure multiple reflections of the light before it leaves the sphere through the exit slit. By so reflecting the light, any nonuniformity of the source which might have been present in the beam is thoroughly eliminated and truly diffuse light is introduced onto the entrance slit of the monochromator. Hence, we are assured duplicity of detector surface illumination without elaborate procedures for lamp positioning. When using the integrating sphere, one can tolerate deviations in lamp positioning of as much as 1/8" to 1/4" which certainly could not otherwise be allowed. A tolerance of ±3° in parallelism of the lamp and entrance slit planes is permissible with the integrating sphere. Without it, as little as 1/2° to 1° would introduce significant error.

Lamp intensity is another critical parameter handled by the integrating sphere. To avoid overloading the detectors, the test lamp energy must be at least 99% attenuated. Approximately 98% of the original lamp energy is lost in the integrating sphere, and 90% of the incident energy on the entrance slit is lost in passing through the monochromator. Thus, only 0.2% of the original lamp energy reaches the detector. For the test lamp, this is a highly desirable figure, but it presents a problem with the standard lamp. Since the standards are several magnitudes of intensity lower than the test lamps, such an extreme attenuation would eliminate nearly all of the energy. The difference in energy levels is accounted for by keeping the standard lamp only a few inches from the

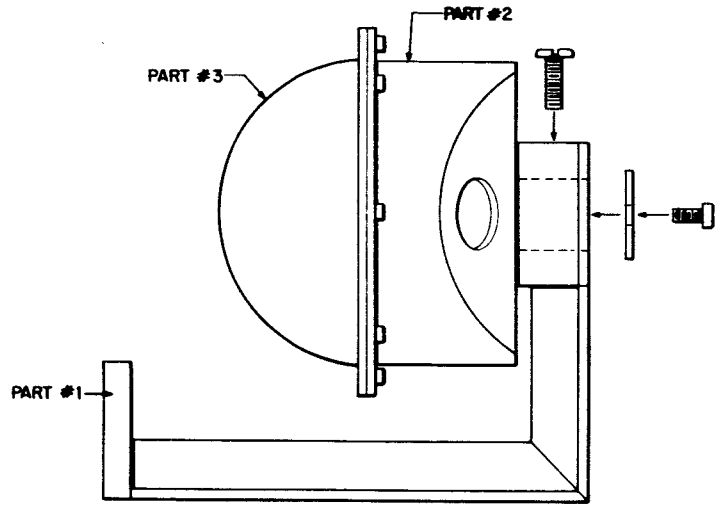

Integrating Sphere Assembly

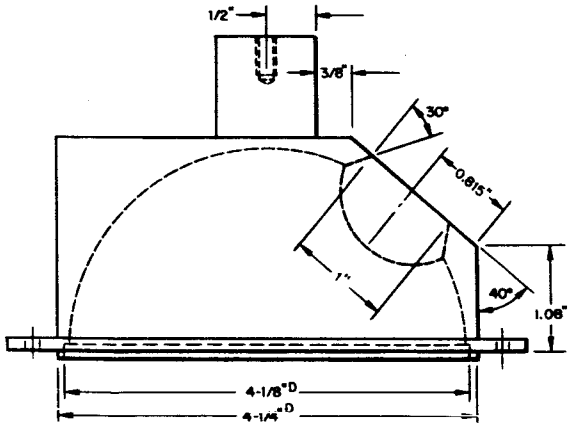

Integrating Sphere Part 2 Horizon. Cross Section

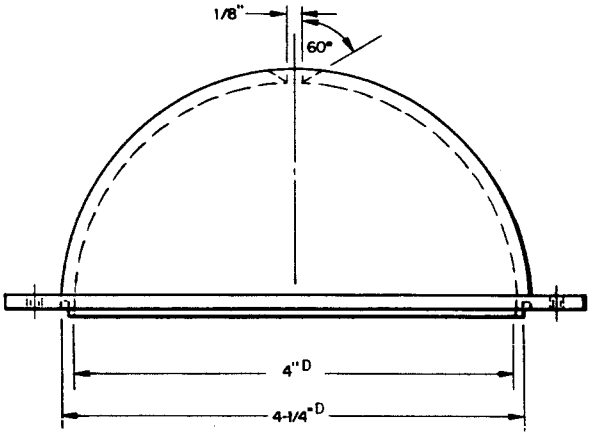

Integrating Sphere Part 3 Horizon. Cross Section

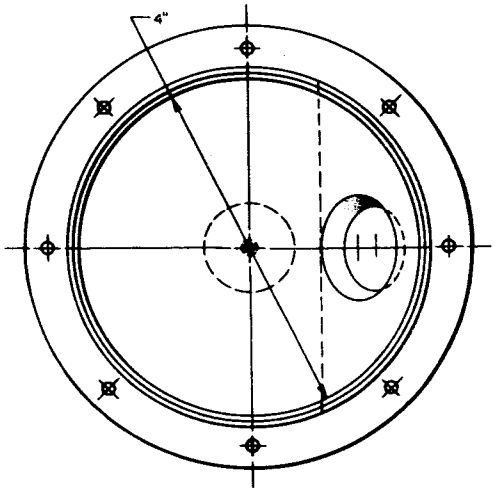

Integrating Sphere Part 2 Vert. Cross Section

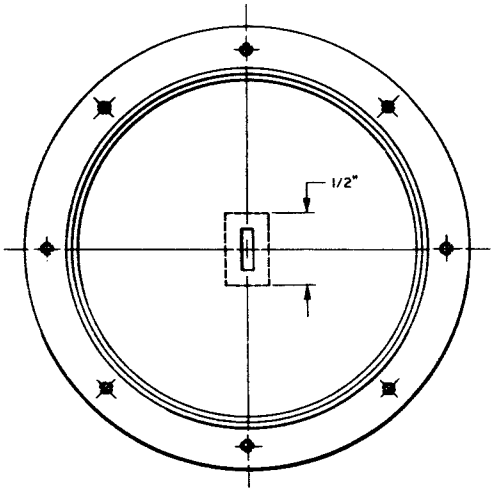

Integrating Sphere Part 3 Vert. Cross Section

Figure 9–Integrating Sphere Specifications

integrating sphere and the test lamp several feet away. In this manner, a very close intensity match throughout the visible and infrared portions of the spectrum is achieved. Since the standard lamps are deficient in ultraviolet energy, the match in this region is poor.

In summation then, the integrating sphere provides four highly desirable advantages:

1. It guarantees repeated, exact detector illumination
2. It reduces detector fatigue and/or saturation
3. It provides a uniform beam of irradiance at the monochromator entrance slit
4. It facilitates a single setting of both test and standard lamp for an entire run.

For detailed information on the Leiss double prism monochromator's per cent transmission and specifications and on the characteristics of the light as it emerges from 'S3' see Figures 10 and 11 and Table 1.

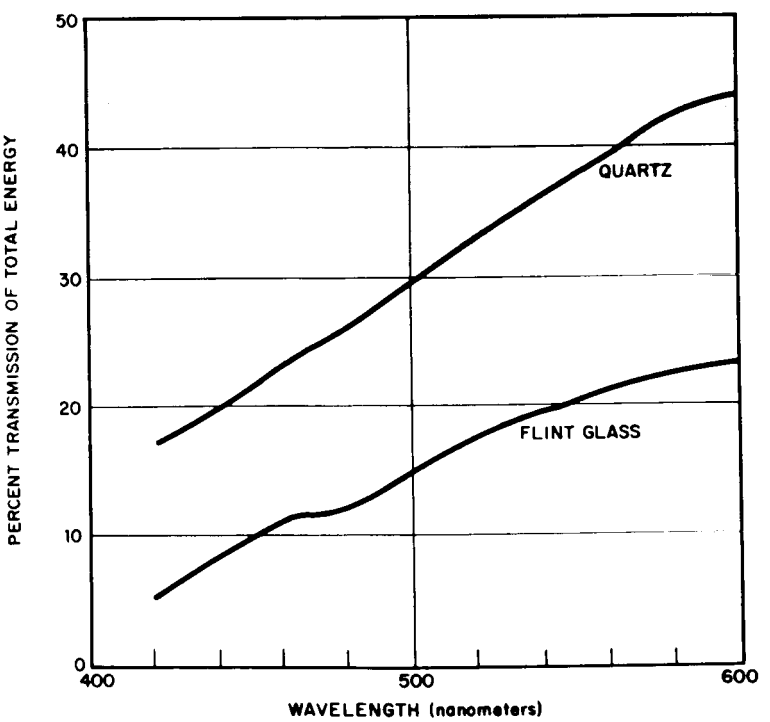

Figure 10–Spectral Transmission of Leiss Double Prism Monochromator

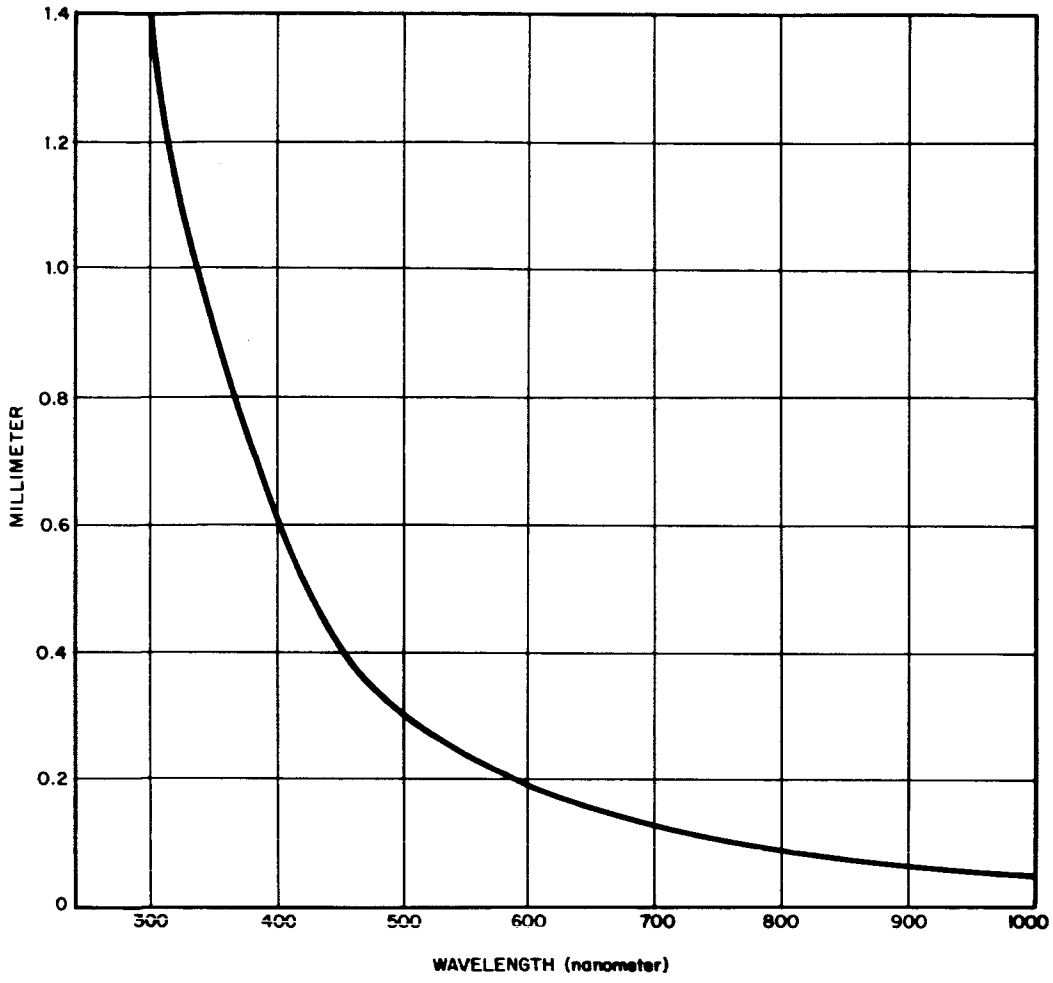

Figure 11—Linear Spread of 5μ Waveband in Plane of Exit Slit-Double Monochromator

The detectors used in this experiment were an R.C.A. type 1P28 Photomultiplier tube, an R.C.A. type 7102 Photomultiplier Tube, and a Lead Sulphide cell. The 1P28 and 7102 have characteristic S5 and S1 responses respectively. Figure 12 is a graph of the spectral ranges of the detectors and their responsivity normalized to the greatest response value and expressed in terms of 100%. The 1P28 and 7102 were powered from a standard d.c. power supply while the PbS cell was powered from two 45 volt dry cell batteries.

The detector output signals were fed into a Brower Laboratories Model 129 Thermocouple Amplifier. Through the aid of narrow-band a.c. signal amplifiers and synchronous rectification of the a.c. signal with the chopper frequency (11.3 c.p.s.), the Brower provides the maximum possible signal to noise ratio. Hence, optimum sensitivity and freedom from the zero drift normally encountered with d.c. coupled detectors is obtained.

Table 1
Specifications of Leiss Monochromator

	Single	Double Prism
Optical System	Prism monochromator with mirror optics	
Prism Material	Exchangeable prisms	
Range of Application with Standard Prisms	200 millimicrons to 20 microns*	
Refracting Angle of Prisms		30°–35°
Prism Dimensions		
Height		50 mm
Length of Hypotenuse		75 mm
Optical Image Formation	Spherical concave mirrors	
Focal Length of Mirrors		300 mm
Useable Surface Area of Mirrors		55 × 57 mm
Effective Relative Aperture		1:6.4 to 1:7.2
Prism Motion	Rotation of finely-graduated wavelength drum, with the aid of worm-and-sector drive, free of backlash. Accuracy of adjustment: 30 seconds	
Linear Dispersion in Exit Slit at λ = 500 millimicrons		
with Flint Glass Prisms		2.4 mm/10 m μ
with Quartz Prisms		0.5 mm/10 m μ
Smallest Resolvable Wavelength Interval at λ = 500 millimicrons		
with Flint Glass Prisms		2.5 AU
with Quartz Prisms		10.0 AU
Spectral Transmission at λ = 550 millimicrons		
with Flint Glass Prisms		20%
with Quartz Prisms		38%
Total Stray Light Effect, produced by radiation more than 10 millimicrons above or below wavelength setting, for flint glass prisms at 500 millimicrons		Less than 1/10,000

*Instrument permits operation above 20 microns. Information on special prisms for range of 20-40 microns on request.

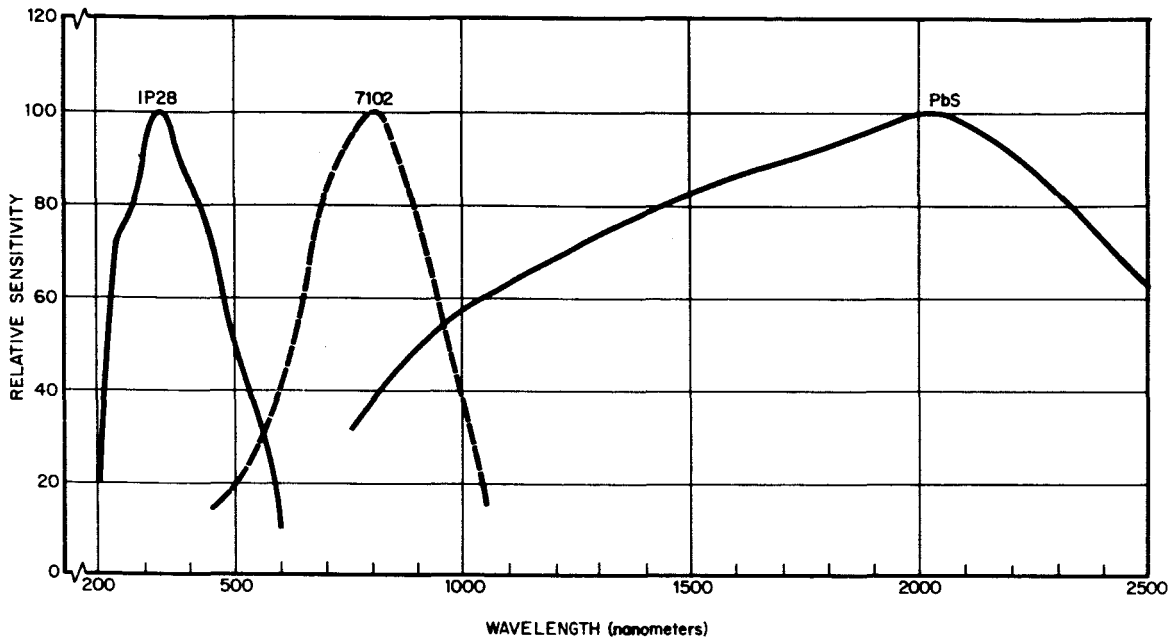

Figure 12–Detector Ranges and Relative Responses

The input signals can be received on any of 21 gain settings, ranging in decade steps of 1, 2.5, and 25 from 0.01 μv to 50 m.v. The input signal is first received by a X200 preamplifier–feedback stabilized–which has a nominal input impedance of 5 megohms shunted by 30 $\mu\mu$F. This unit incorporates a low noise input tube, with all d.c. supply voltages regulated, giving full meter deflection with one μv peak-to-peak input signal. The preamplifier is followed by a X5,000 main amplifier. A "twin tee" filter limits the amplifier bandwidth to provide optimum signal to noise ratio at each chopping frequency. Any noise pulses greater than 25 times the maximum are handled without distortion thus enabling integration to be performed in the output stage without introducing error. The amplifier bandwidth is controlled by the response time switch which has six settings from 0.1 sec. to 30 sec. The optimum setting is dependent upon the signal to noise ratios and chopper frequency. A strong signal chopped at 11.3 c.p.s. is best handled between 0.1 sec. and 1.0 sec. Weaker signals require longer integrating times.

The d.c. output signal can be read from the Brower's 1% mirror-scale, 5" panel meter (1 volt full scale) or relayed to an external recorder.

The data logging system used for this experiment was a Control Equipment Corp.'s Model #1066 Spectrometer Data Logger. It was manufactured under contract with the Radiometry Group specifically for spectrometric measurements. Figure 13 is a block diagram of the system.

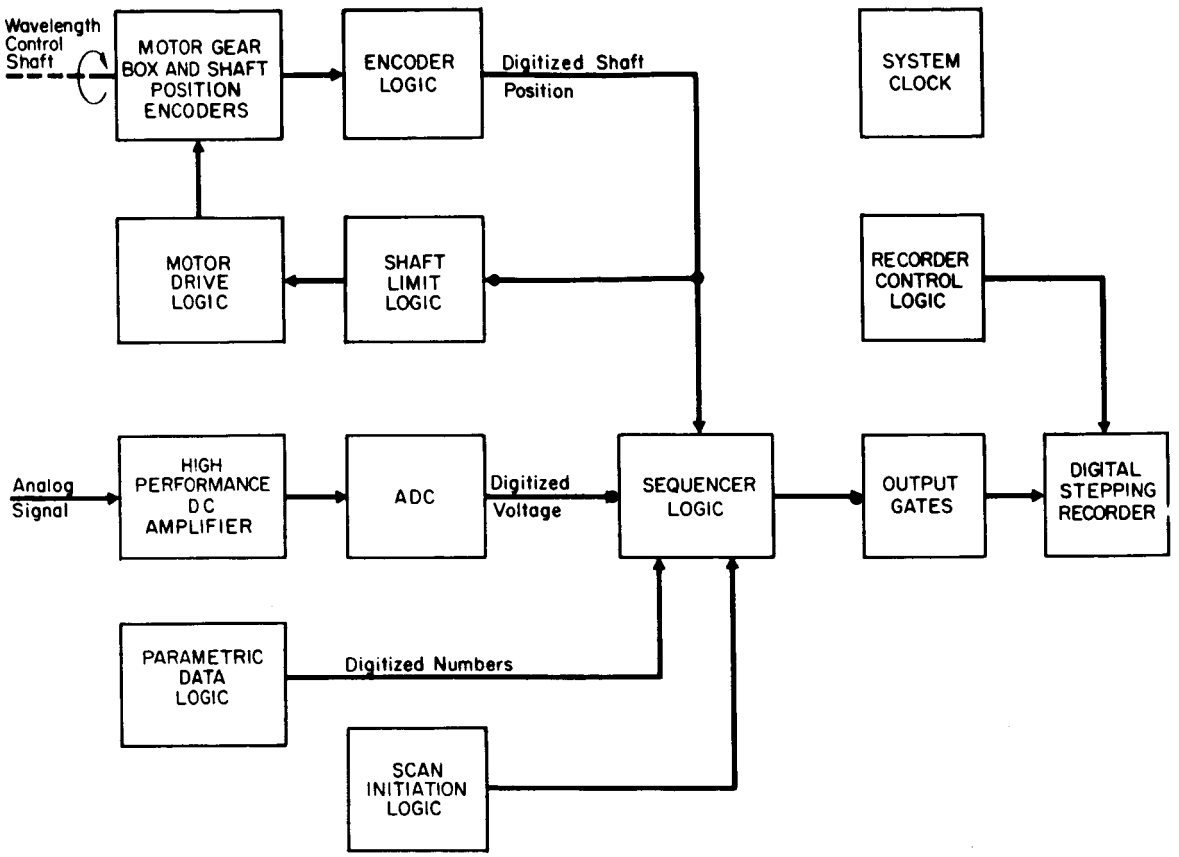

Figure 13–Functional Block Diagram of Spectrometer Data Logger

This instrument performs several functions. It contains a motor and gear box which drive the monochromator wavelength drum. The motor drive logic controls the direction and speed of the stepping motor as determined by the Motor Control panel array on the front of the data logger (Figure 14). Motor operation is in three modes: reverse, neutral, forward. The speeds are 1/5, 1/10, 1/20, and 1/40 r.p.m. The motor drives the gear box which in turn drives the logger's wavelength control shaft and two photoelectric shaft position encoders. These continuously monitor the angular position of the shaft and the number of revolutions it has made from zero reference. The wavelength control shaft is quantized into 2,048 angular parts per revolution–14 revolutions maximum. Each of the 28,672 shaft positions (2,048 × 14) can be accurately reproduced any number of times to within ±1 L.S.B. (least significant bit). The shaft position is displayed in digital form on the front control panel of the data logger and is constantly monitored by the shaft limit logic. When the shaft reaches the zero revolution or 14th revolution position, the shaft limit logic stops the motor and illuminates the proper maximum or minimum indicator lamp (situated on either side of the Motor Control array).

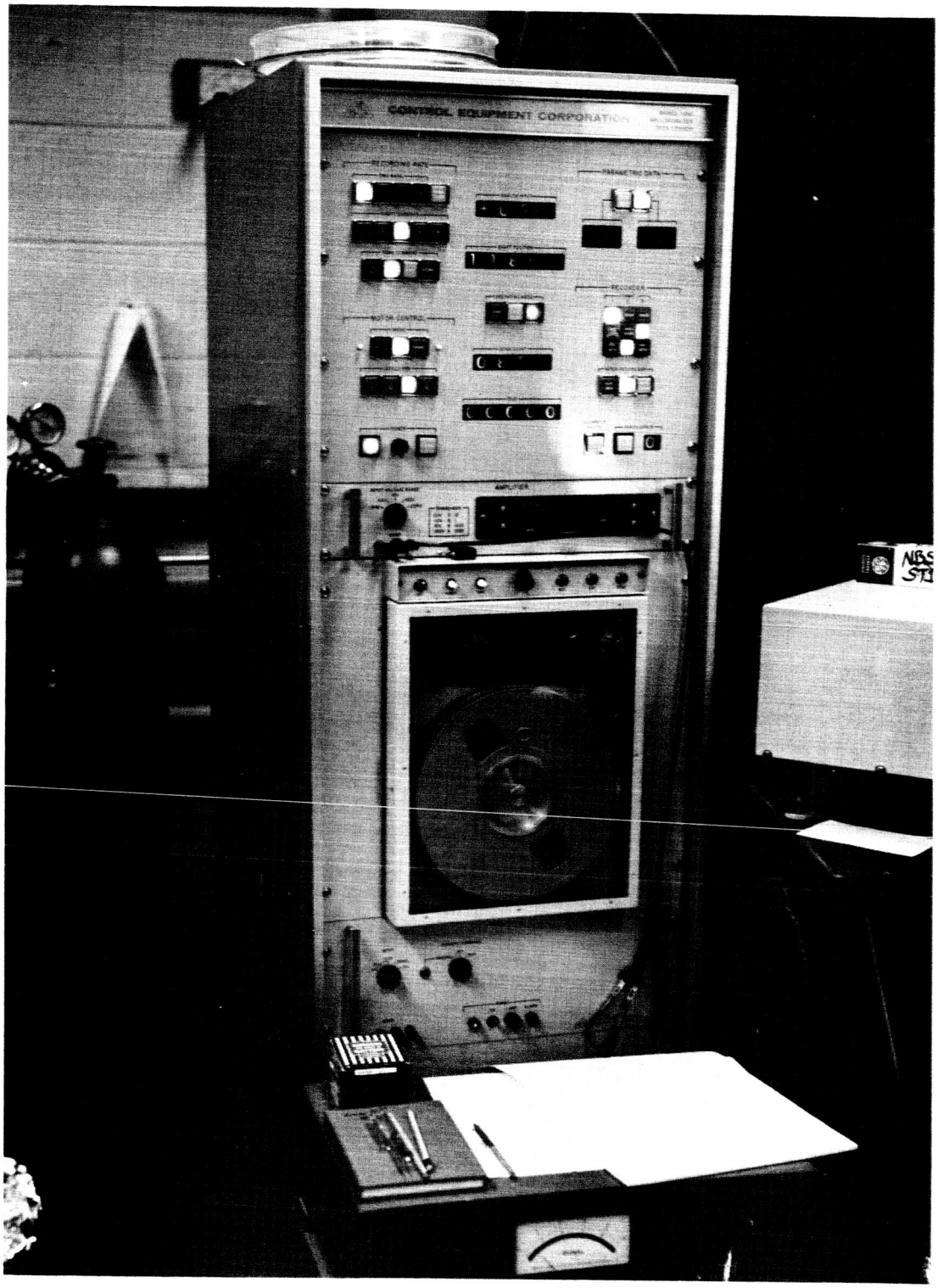

Figure 14–Spectrometer Data Logger and Brower Amplifier

Parameters are designated by the two 3 digit thumbwheel switches located in the upper right corner of the control panel. For this experiment, gain changes were made with the Brower (lower foreground in Figure 14) though they can be effected by the data logger. The Brower was chosen because its accuracy and range of operation are better than the data logger's. However, to be recorded on the magnetic tape, the gain changes had to be indicated on the Parametric Data panel array.

Located in the upper right corner of the front control panel is the Recording Rate array which controls the scan initiation logic. Scan commands can be initiated on a time base, shaft position, manual, or external basis. On time base, scans can be initiated in decade steps from one every 1/10th second to one every 100 seconds, on shaft position–at every shaft position, every 2nd, 4th, 8th, or 16th position. The manual and external command modes are self explanatory.

Upon receiving a pulse from the scan initiation logic, the sequencer records three inputs (analog voltage, shaft position, parametric data) on magnetic tape in the sequence dictated by the Recorder Format array. An inter-record gap (3/4" of blank tape) can be generated automatically or manually. Automatically–one is generated after each scan. The data logger's electrical specifications are listed in Table 2.

The rapid, frequent gain changes necessitated by the instability and heavy U.V. emission spectra of the carbon arc were easily handled with this system. Many errors in data acquisition inherent in strip chart recording methods were avoided by using the data logger.

The beam scanning device used for this experiment was designed by A. J. Hobbs of the Radiometry Group for use in conjunction with a large simulator operated by the group. Though not an optimum instrument for such a small beam as that of the carbon arc, it was none-the-less found to be readily adaptable to this project. Figure 15 is a full view of the scanning system being used with the large simulator.

Figures 16 and 17 display some of the characteristics of this scanning system. Because the intensity was measured with a solar cell, the uniformity scans cover a limited spectral region. This, however, is not a necessary condition for uniformity measurements. The pyrheliometer used to calculate the intensity values is a broad-band detector. The radial arm on which a small solar cell is mounted (Figure 18) was detached from its support apparatus and placed on an adjustable table. The scanner was then wired to a x-y plotter which graphed the beam intensity as a function of position within the beam. The ratio of solar cell travel to plotter arm travel was 16" to 14". Thus, the resulting graphs are

Table 2
Spectrometer Data Logger Specifications

Analog Input

Type: differential, with guard shield.
Full-scale ranges: ±0.1 vdc
±1.0 vdc
±10 vdc
±100 vdc

Impedance: 10 megohms
Common mode rejection (0.1 volt scale): 100 db, dc to 60 cps
Accuracy of A/D conversion: ±0.1% ±1/2 LSB

Wavelength Control Shaft Input

Type: geared photo-electric encoders
Quantization: 2,048 parts per revolution
Shaft motion: 14 revolutions max
Accuracy of quantization: ±1 LSB

Wavelength Control Shaft Drive

Type: stepping motor – gear box, bidirectional.
Speeds: 1/5, 1/10, 1/20, and 1/40 RPM
Speed accuracy: ±0.01%
Limit stops: electronic stops backed up by cam switch stops.
Manual operation: electric clutch permits disconnecting output shaft from gear train without disconnecting encoders.

Recorder

Type: Digi-Data Model 1420 stepping recorder
Tape width: 1/2"
Packing factor: 556 bits per inch
Stepping rate: 0 to 200 steps per second
Format: 7-track, IBM-compatible
Reels: 10-1/2" IBM-type reels
Inter-record gap: 3/4", high-speed to minimize data loss
Parity generation: parity generated within recorder; longitudinal check character is recorded when IR gap is commanded.

For complete recorder specifications, see "Operation and Maintenance Manual for Digi-Data DSR 1400 Series Digital Stepping Recorders."

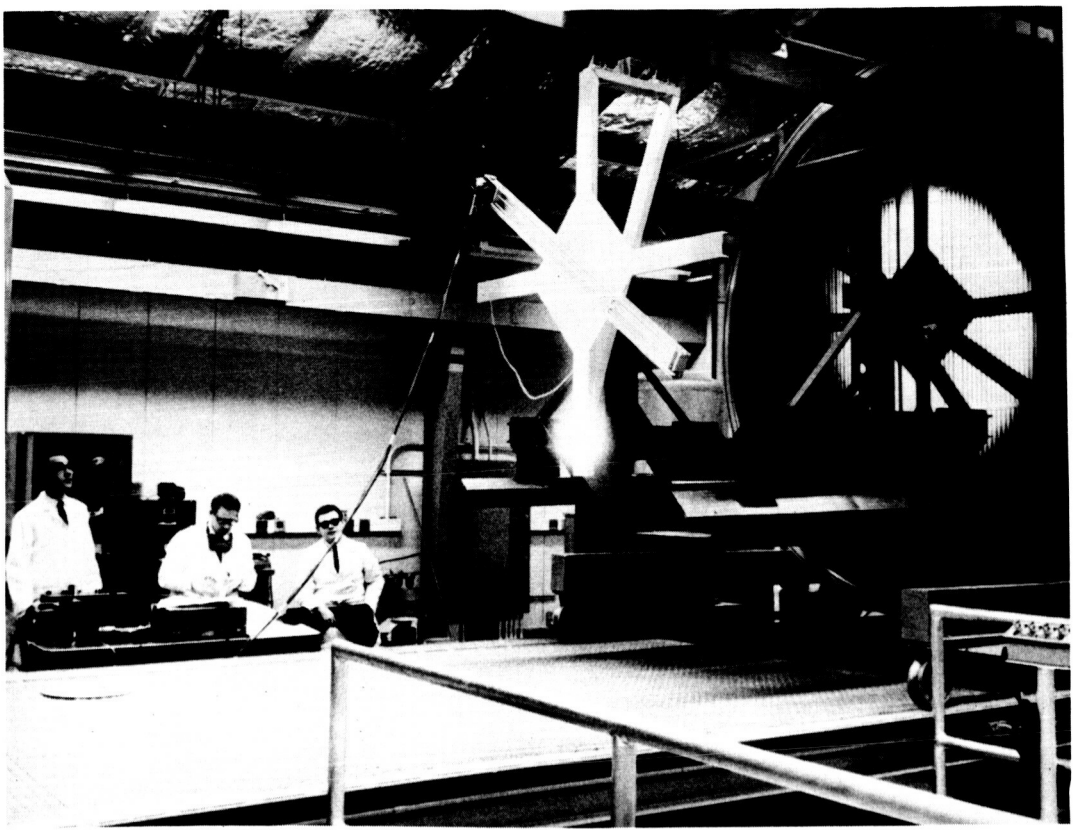

Figure 15–Uniformity Scanning Device and Support Structure

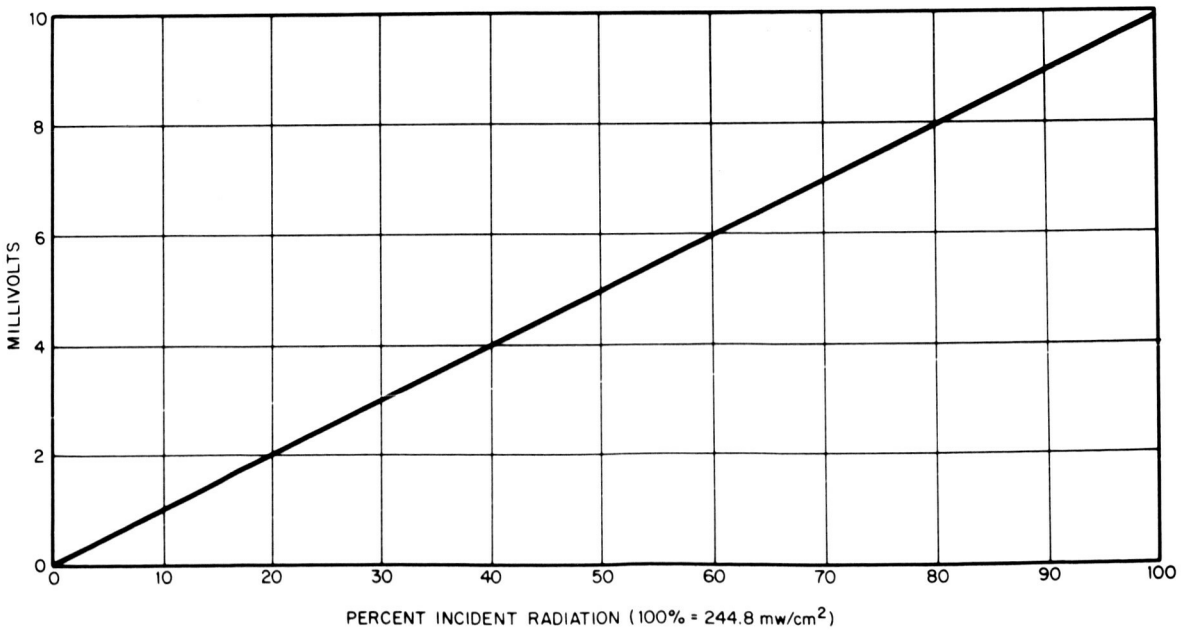

Figure 16–Scanning System Output

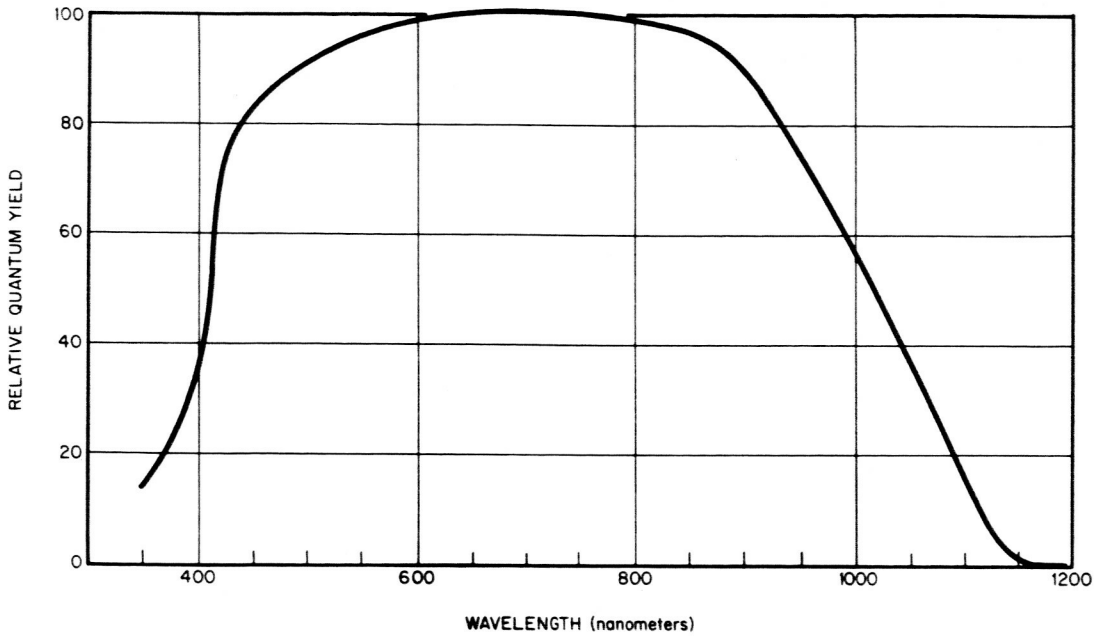

Figure 17–Solar Cell Responsivity

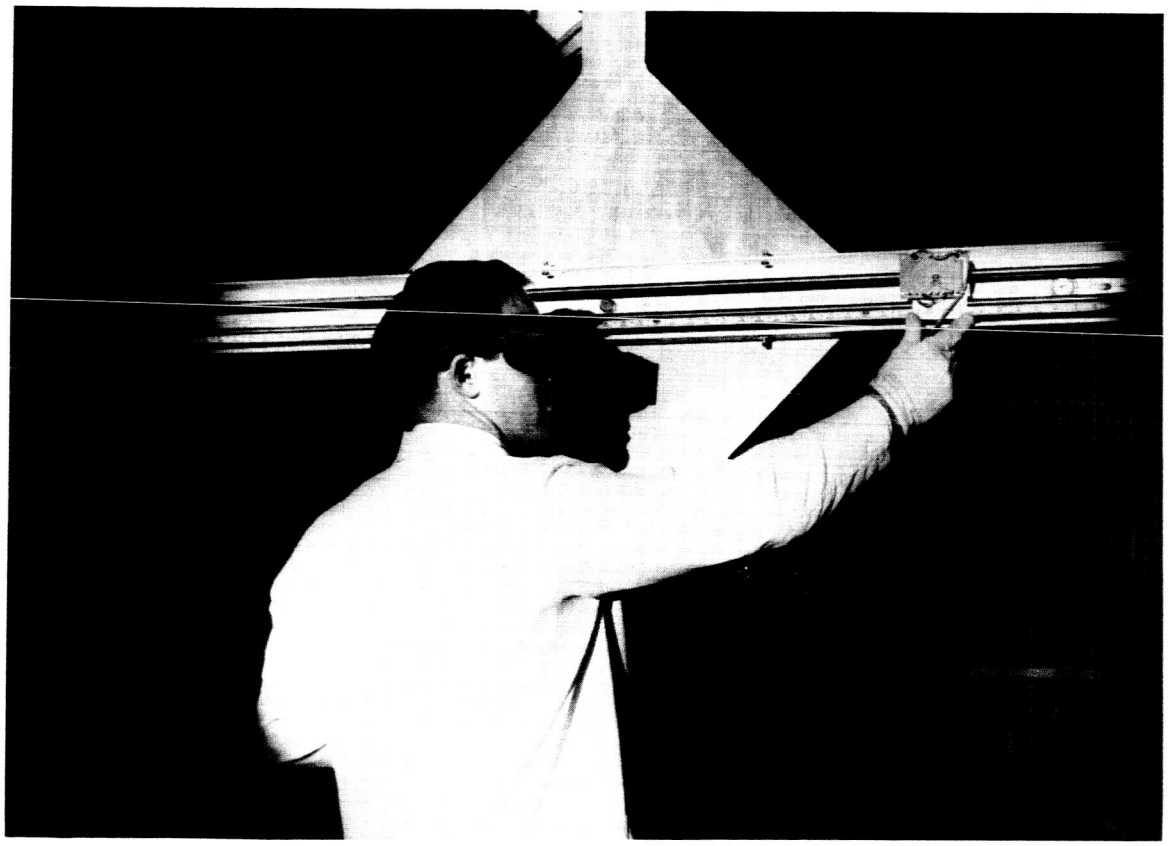

Figure 18–Uniformity Scanning Device Closeup of Mobile Solar Cell

horizontally scaled by a factor of 1.14" to 1". The plotter pen sensitivity, accurate to within ±0.05 m.v., was set at 1 m.v. input stimulus per inch of pen travel. Figure 16 is a graph of the scanner systems output in m.v. as a function of incident radiation upon the solar cell. 100% on this graph is equal to 100% on the uniformity scans (Figures 24-33) – 244.8 mw/cm^2 or 1.8 solar constants.

A pinhole device (Figure 19) was used to measure the arc's half angle collimation. This device was also designed by A. J. Hobbs, the group's mechanical engineer. It was calibrated against the sun for this experiment. An Eppley normal incidence pyrheliometer, recalibrated at Table Mountain, Calif. for 100 mw/cm^2 irradiation was employed to measure the arc's intensity. A reading was taken at the center of each scan. From various computations and scaling of the scans as shown, the degree of accuracy of these measurements was proven to be within a range of ±1.29 mw/cm^2 or 0.0095 solar constants.

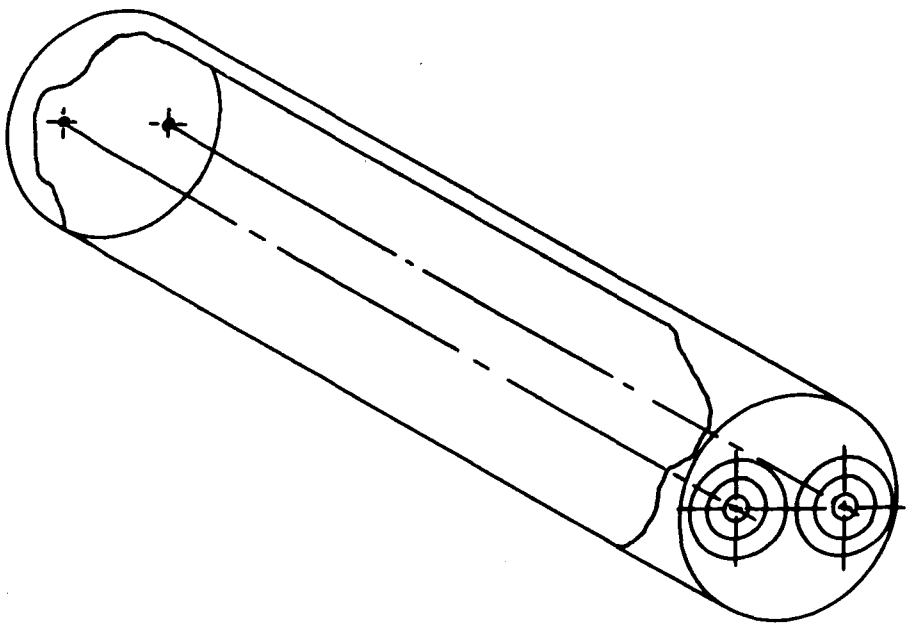

Figure 19–Collimation Angle Measuring Device – Diagram

OPERATIONAL PROCEDURES

Two spectral distribution measurements of the carbon arc were taken, one with and one without the collimating lens. This was done to provide accurate data on the lens' transmission, quality, and any spectral distortions it might cause. The data were taken on two successive days with room conditions, lighting, lamp positions, and other various parameters as well controlled as possible.

The lab walls were painted black and black curtains were drawn about the arc and experiment apparatus to minimize reflections. An iris mechanism was employed to shield the monochromator body from the beam and expose only the integrating sphere. For this run, the iris was set to pass a beam of about 6" in diameter. Of this beam we used only the very top portions as can be seen from Figure 20.

Figure 20–Monochromator and Integrating Sphere in Use

Normally, when using the integrating sphere, the test lamp can be operated continuously without interferring with data from the standard lamp simply by rotating the integrating sphere. This also permits, as mentioned before, a single setting of the standard lamp. Hence, any probable test or standard lamp parameters affected by temporary shut down are abrogated. In this instance, however, lack of space dictated a single integrating sphere setting. Arc operation, therefore, had to suspended while test lamp data were being taken.

The spectral distribution measurements were taken from 250 nm to 2500 nm. This was divided into four sections as dictated by the range capabilities of the Brower amplifier. The first was from approximately 250 nm to 335 nm using the 1P28 Photomultiplier Tube at 1200 d.c. volts input. The second section, 320 nm to 640 nm, was scanned using the 1P28 at 600 volts input. By varying the gain of the detector amplifier in this manner, thus decreasing the overall diode voltage, the detector's quantum yield – i.e. electrons per photon efficiency – can be effectively reduced. The 7102 Photomultiplier was employed from 550 nm to 1100 nm at 1200 volts. The region from 880 nm to 2500 nm was scanned with the PbS cell powered by two 45 volt dry cell batteries. In the regions of change from one detector mode to another, overlaps of 15, 85, and 220 nm, respectively, were allowed.

The beam uniformity measurements were taken in two sets, linear and temporal, on the same day. The arc was left in continuous operation. One obstacle to accurate uniformity measurements which presented quite a problem was a constant shift in beam diameter. The collimating lens and lens housing imposed a maximum diameter of 12", but wide deviations below this were observed. The greatest deviation noted was 9", but the average seemed to be about 10-1/2" to 11". Because of this shift in diameter, it was decided that 16" linear scans would provide better data than 12" scans. No relative periodicity nor any unusual phenomena was observed. The problem, on the contrary, would seem to be one inherent in the arc itself. It is likely that, at times, the positive carbon advancement was too great and the burning carbon tip was thrust forward past the focal point of the collimating lens. This would cause a divergent beam to emerge from the lens. For commercial purposes this flow is unimportant; but for the purposes of solar simulation, it presents a significant barrier. Accurate predictions and/or control of test volume irradiance are impossible under such conditions.

The linear uniformity scans are taken in a plane 43" from the collimating lens and 64" from the arc as shown in Figure 21. Each scan took 2-1/2 minutes to complete and the entire run of 10 took 55 minutes. The temporal scans were taken in the same plane at five points within the beam (Figure 21). Each scan took 3 minutes to complete and the full set required 25 minutes. Because the x-y plotter module was changed from high sensitivity to time base, the scaling of the graphs is not the same. Neither is the accuracy of the measurements as good; i.e., ±0.5%.

The collimation angle measuring device and the pyrheliometer are shown in Figure 22, as they were used.

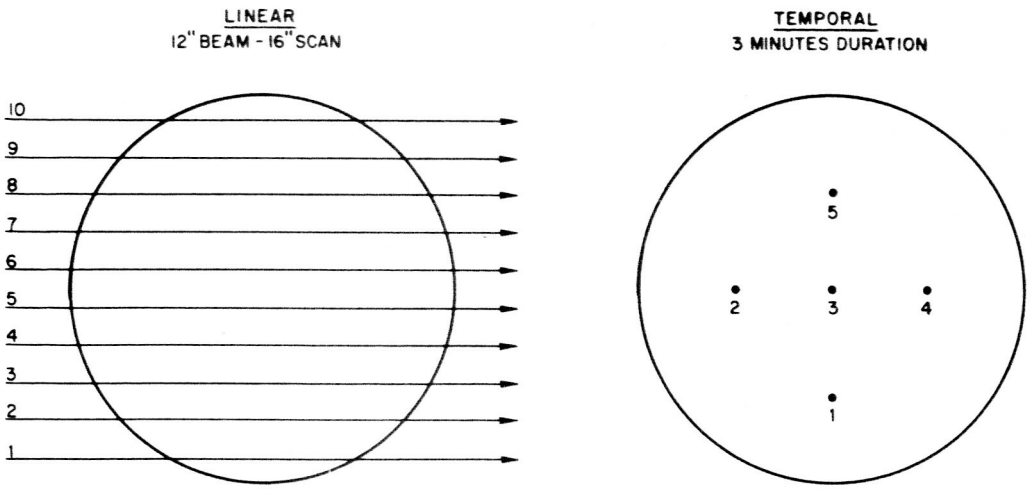

Figure 21–Linear and Temporal Scan Positions

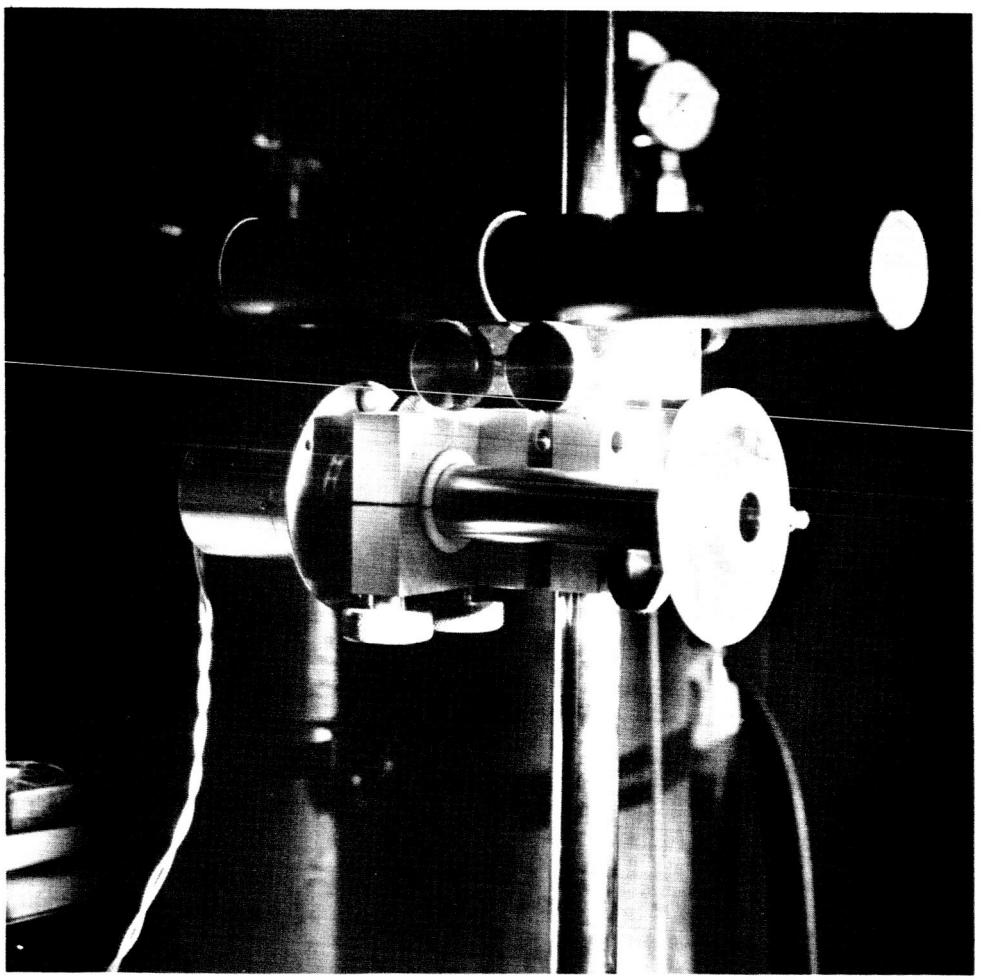

Figure 22–Collimation Angle Measuring Device and Pyrheliometer in Use

DATA REDUCTION AND INTERPRETATION

Some general conception of beam uniformity is shown by Figures 23-32, the linear uniformity graphs. You will note from scans 3 through 6 that the greatest intensity deficiency occurs at beam center while the peripheral areas are replete with energy. However, the corresponding areas of scans 6 through 9 show radical differences. Though intensity decreases above beam center, uniformity greatly increases. The extreme deficiency at beam center is caused by the shadowing effect of the negative carbon and would seem to be an immutable obstacle to be lived with rather than corrected.

The temporal stability scans (Figures 33-34) indicate an almost definite periodicity over longer time periods with very little deviation from same. This, like the beam diameter, is a function of the positive carbon advancement and has such periodicity because the positive carbon consumption rate is very regular but the carbon protrusion control is not.

Figure 35 is a chart of the average intensity per 1.6" square block with a beam diameter of 12". Values for some areas not included in the beam proper have been given to illustrate the extreme instability and nonuniformity of the arc. This energy is directly attributed to the tail flame. Energy contributions from the flame are heavy and concentrated in the lower half of the beam (Figure 24). From scans 1-5, it can be seen that this half is considerably more noisy than the upper half-especially so in the periphery. Beginning at scan 6, the beam is much quieter. A comparison of scans 1 and 10, which by the rules of simple logic should be much the same, along with the information discussed above reveals the following:

1. The noise is legitimately a part of the beam and not attributable to the solar cell or plotter.
2. The lowest 1/10th of the beam is much more intense than the highest 1/10th and much less uniform.
3. The tail flame is responsible for both increased intensity – high desirable – and increased instability – highly undesirable. The instability contributed by the tail flame is only 25% of the total, however. The remaining 75% is inherent in the arc.

Figures 36 and 37 represent the spectral irradiance of the arc with and without the collimating lens. Figure 38 is a plot of the air mass zero solar irradiance presented in the same manner.[1] The bare arc shows an excess of

[1] Johnson, F.S., "The Solar Constant," J. of Met., Vol XI, No. 6, Dec. 1954.

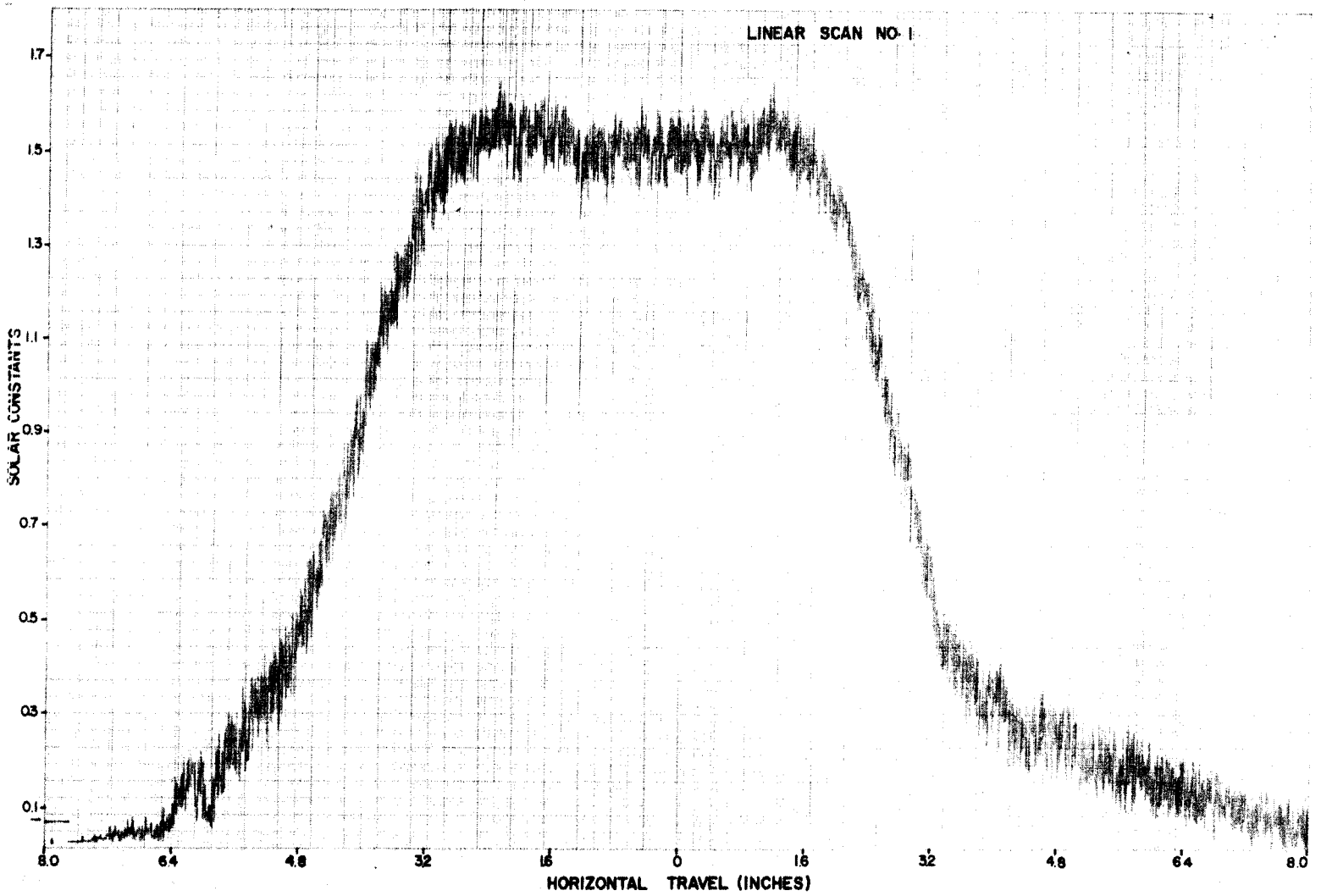

Figure 23–Linear Uniformity Scans

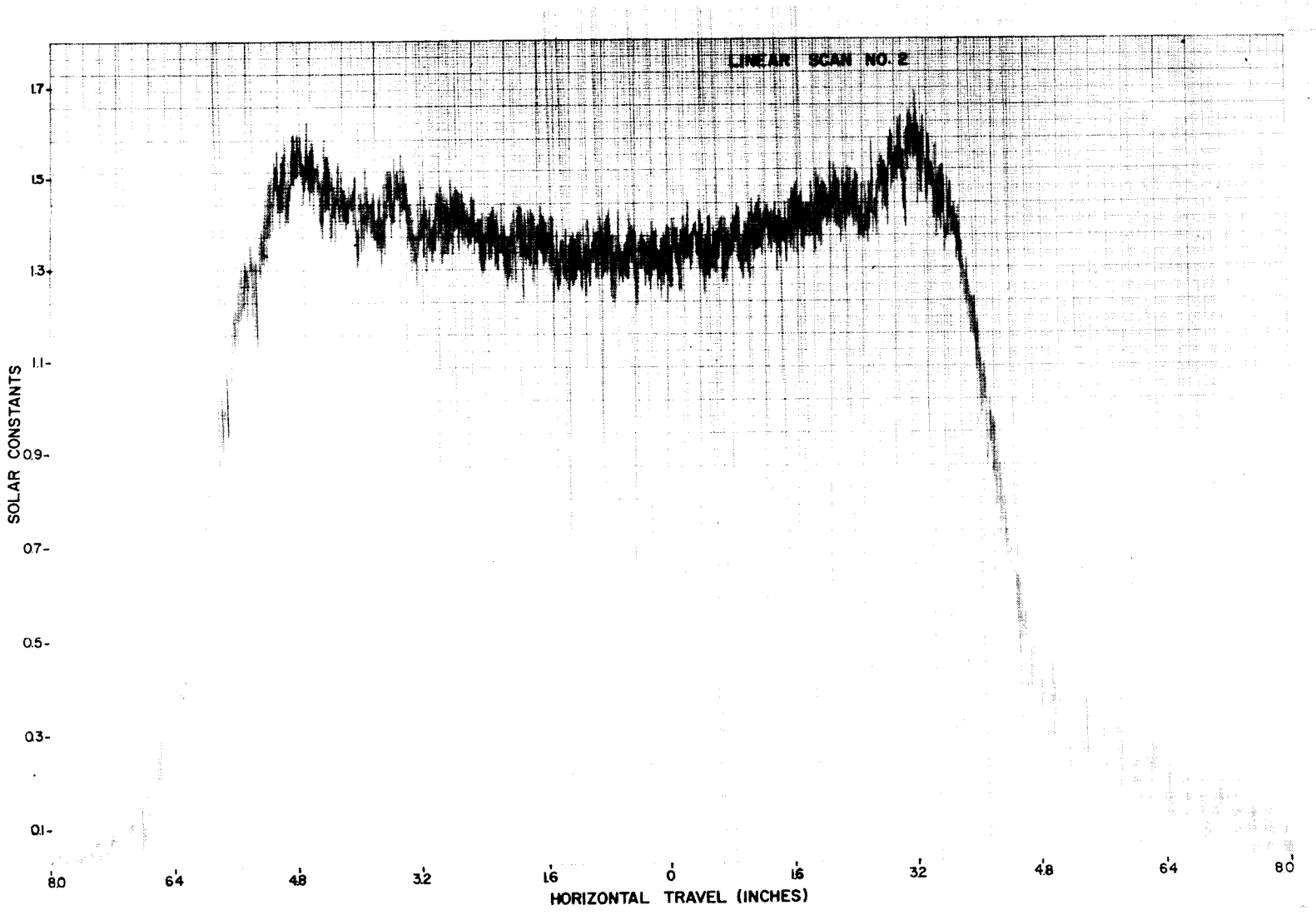

Figure 24–Linear Uniformity Scans

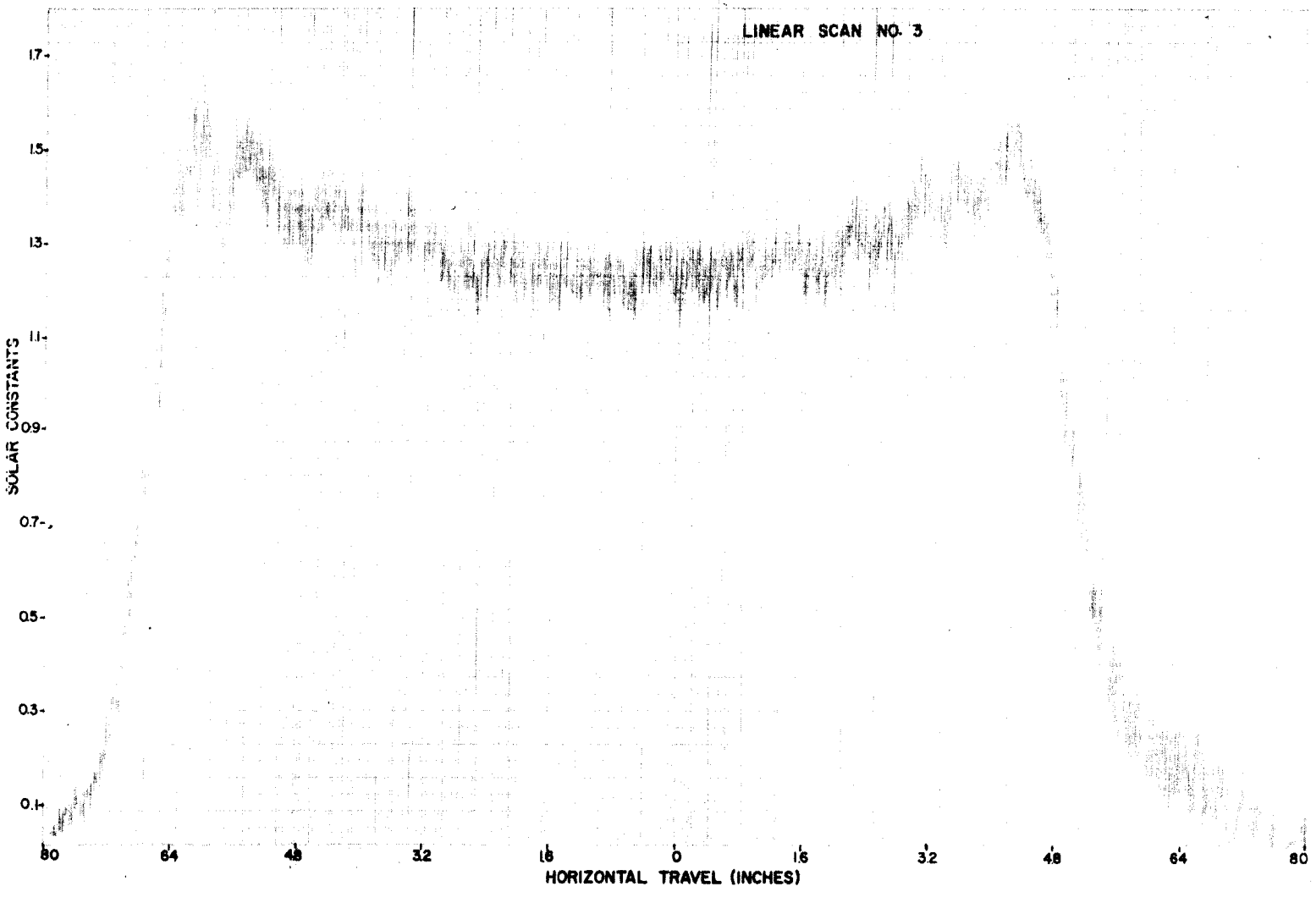

Figure 25–Linear Uniformity Scans

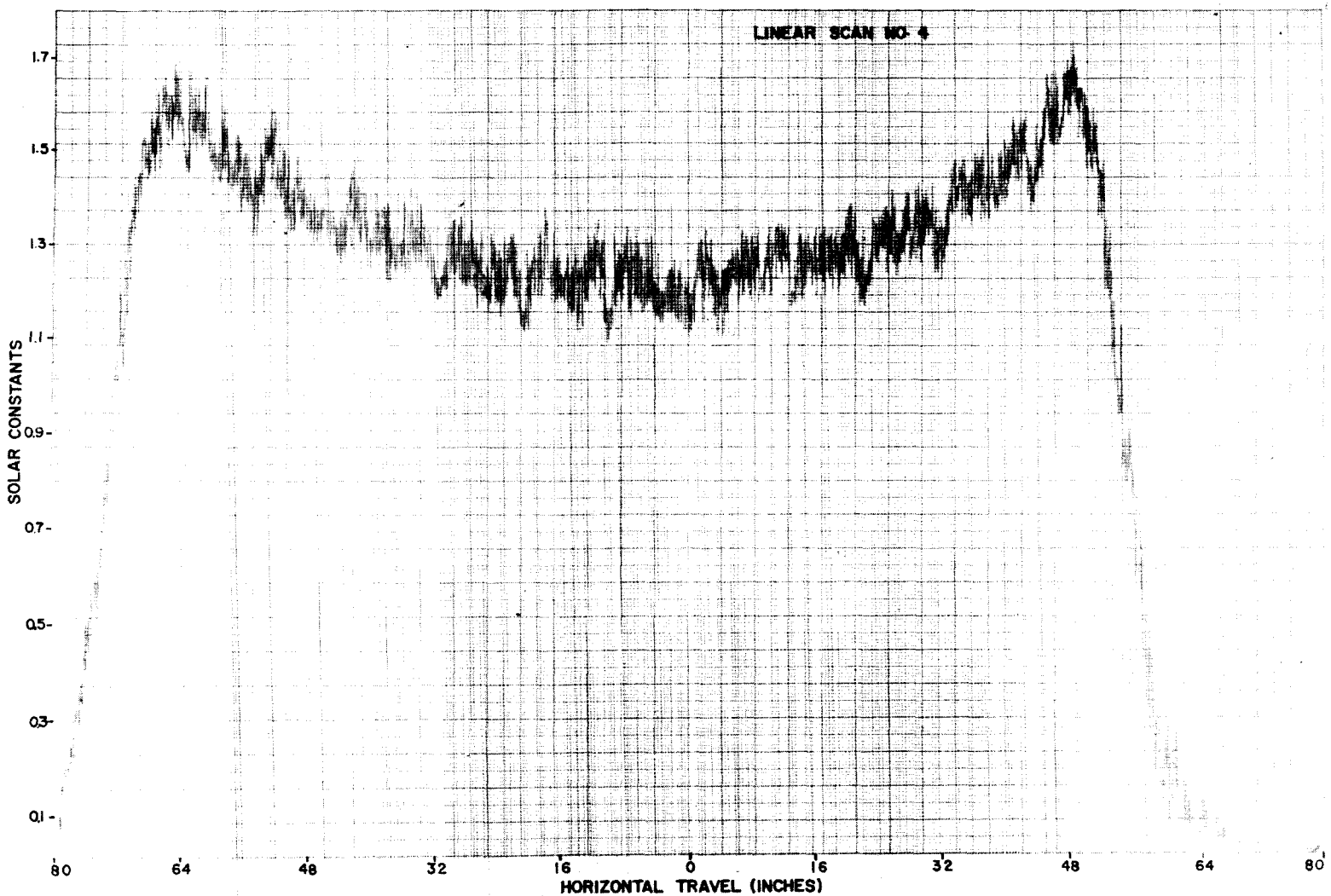

Figure 26–Linear Uniformity Scans

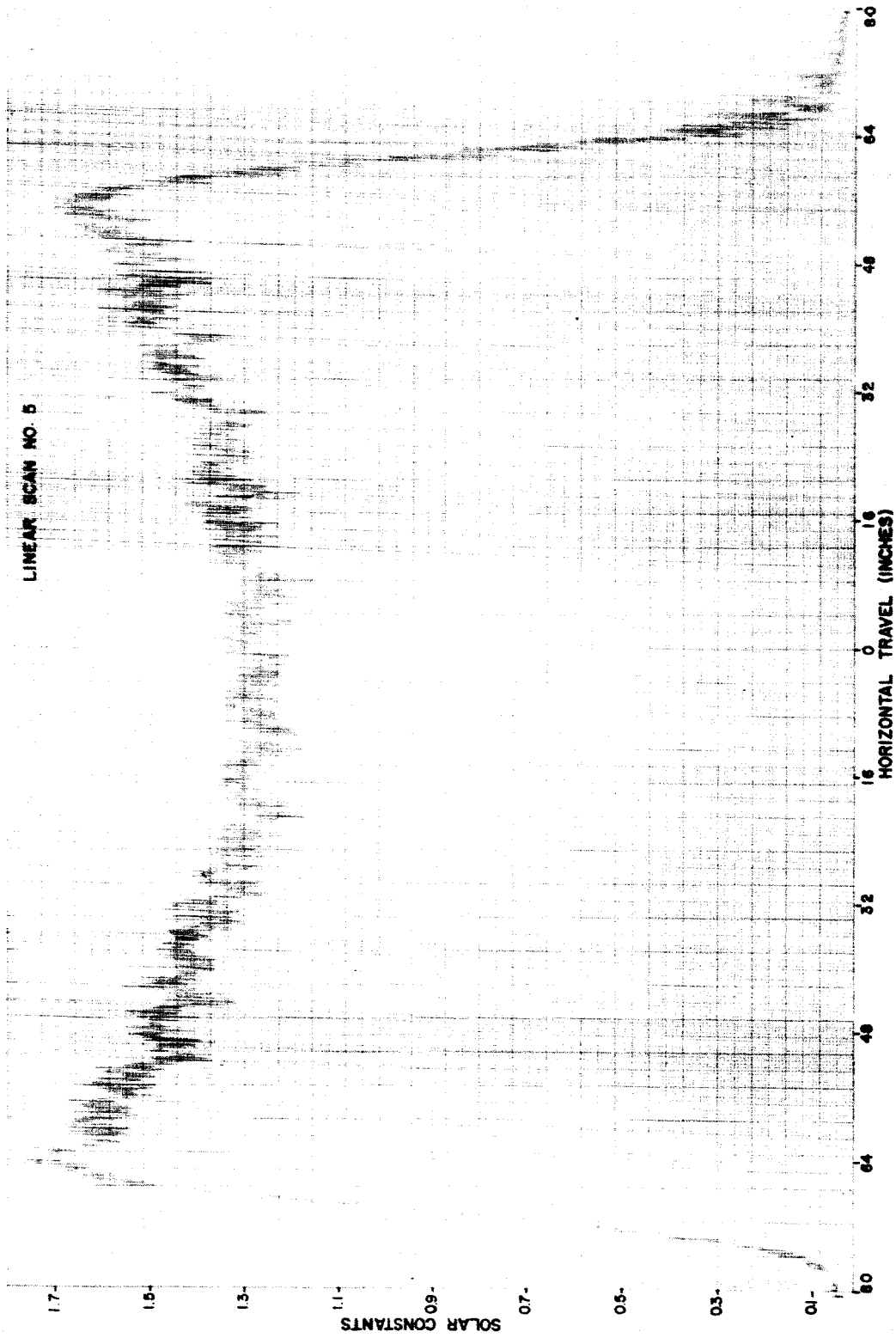

Figure 27–Linear Uniformity Scans

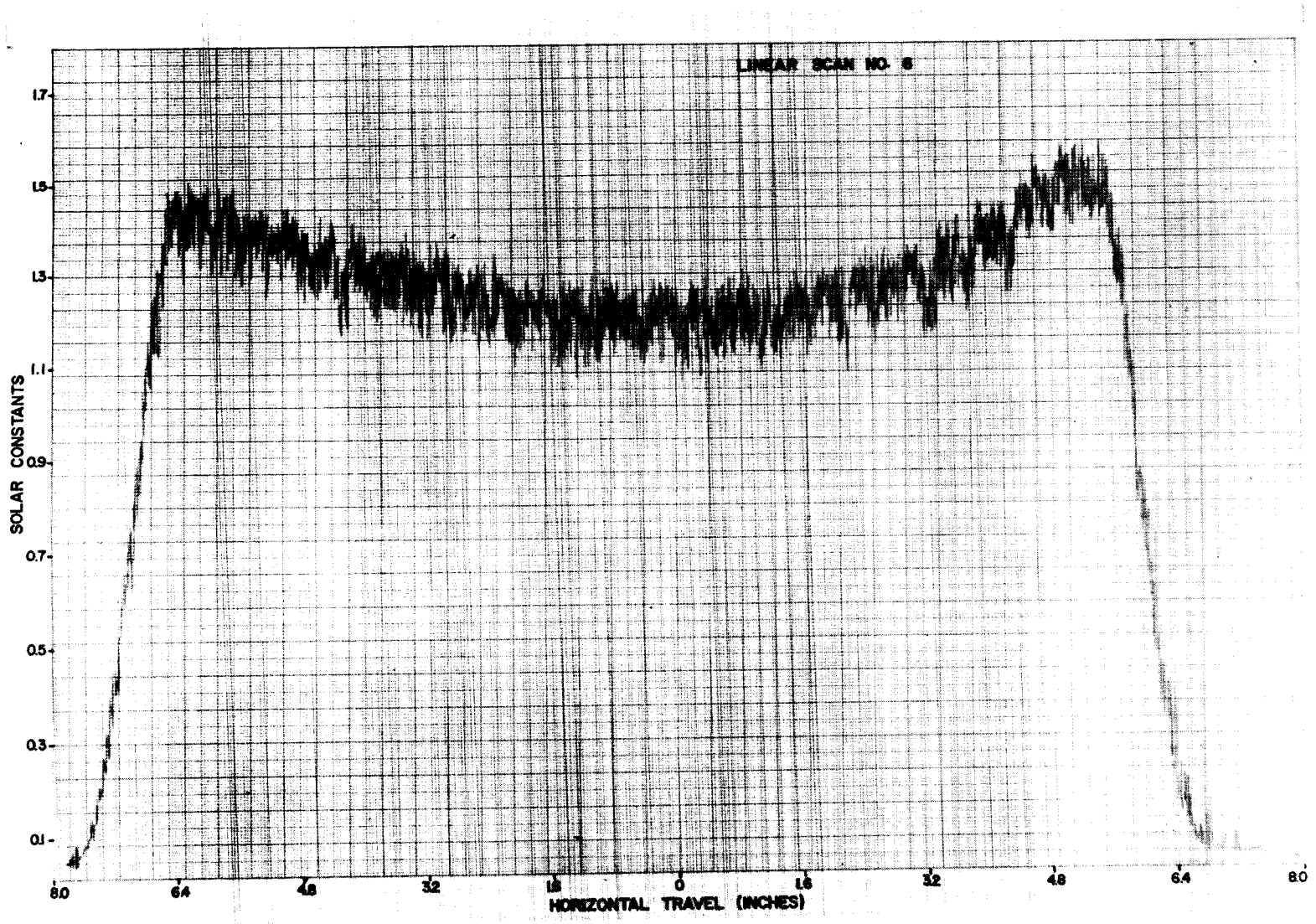

Figure 28–Linear Uniformity Scans

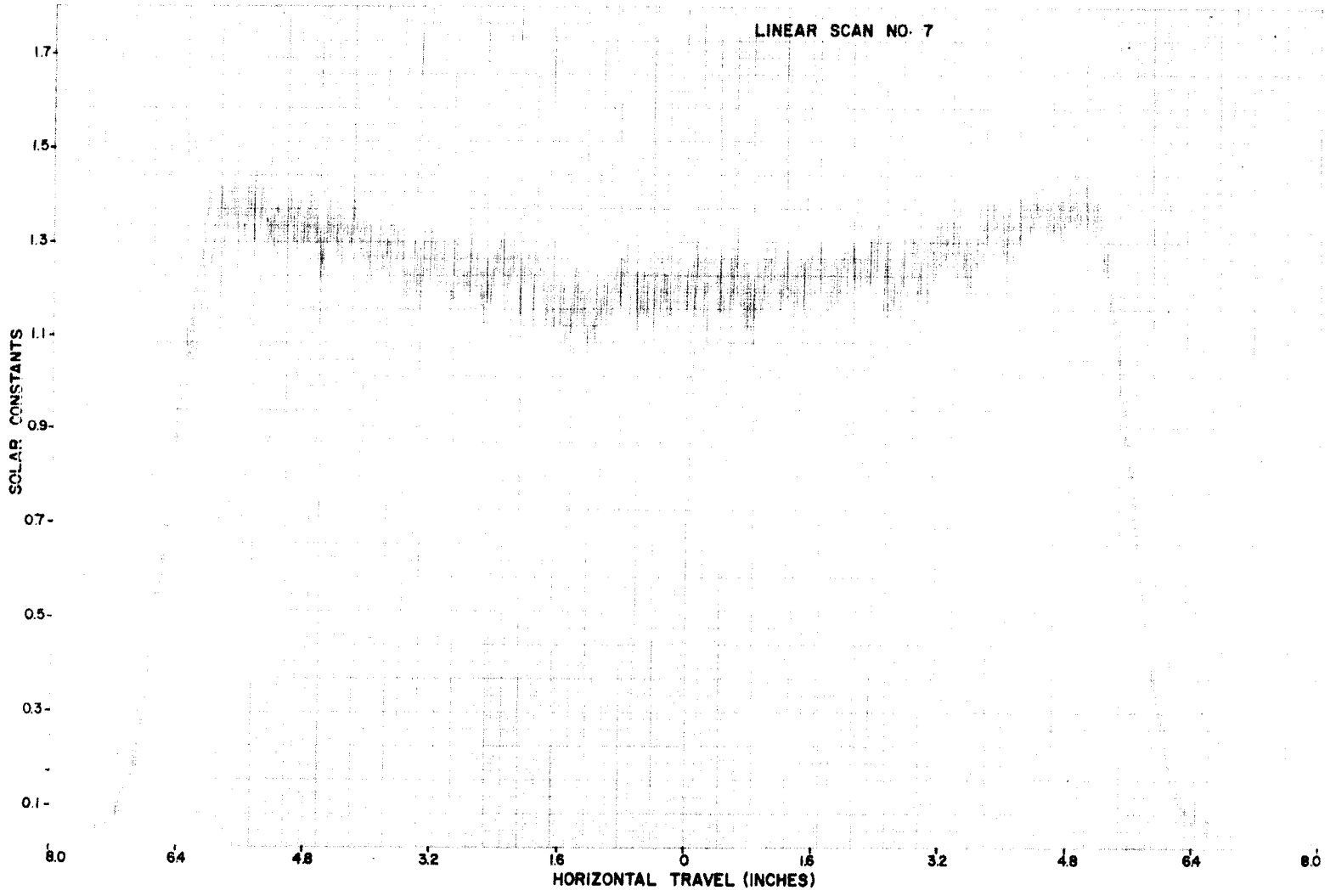

Figure 29–Linear Uniformity Scans

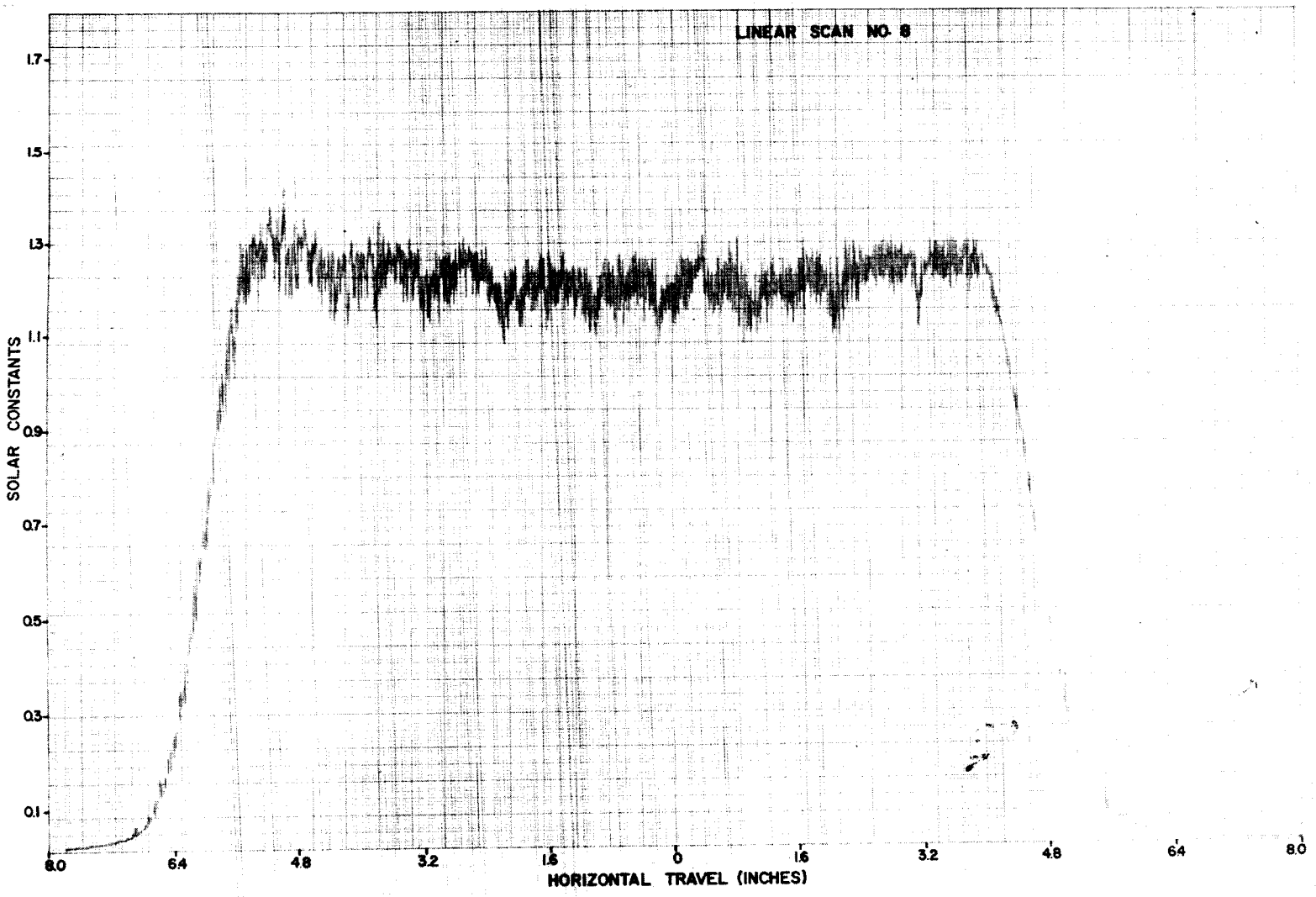

Figure 30–Linear Uniformity Scans

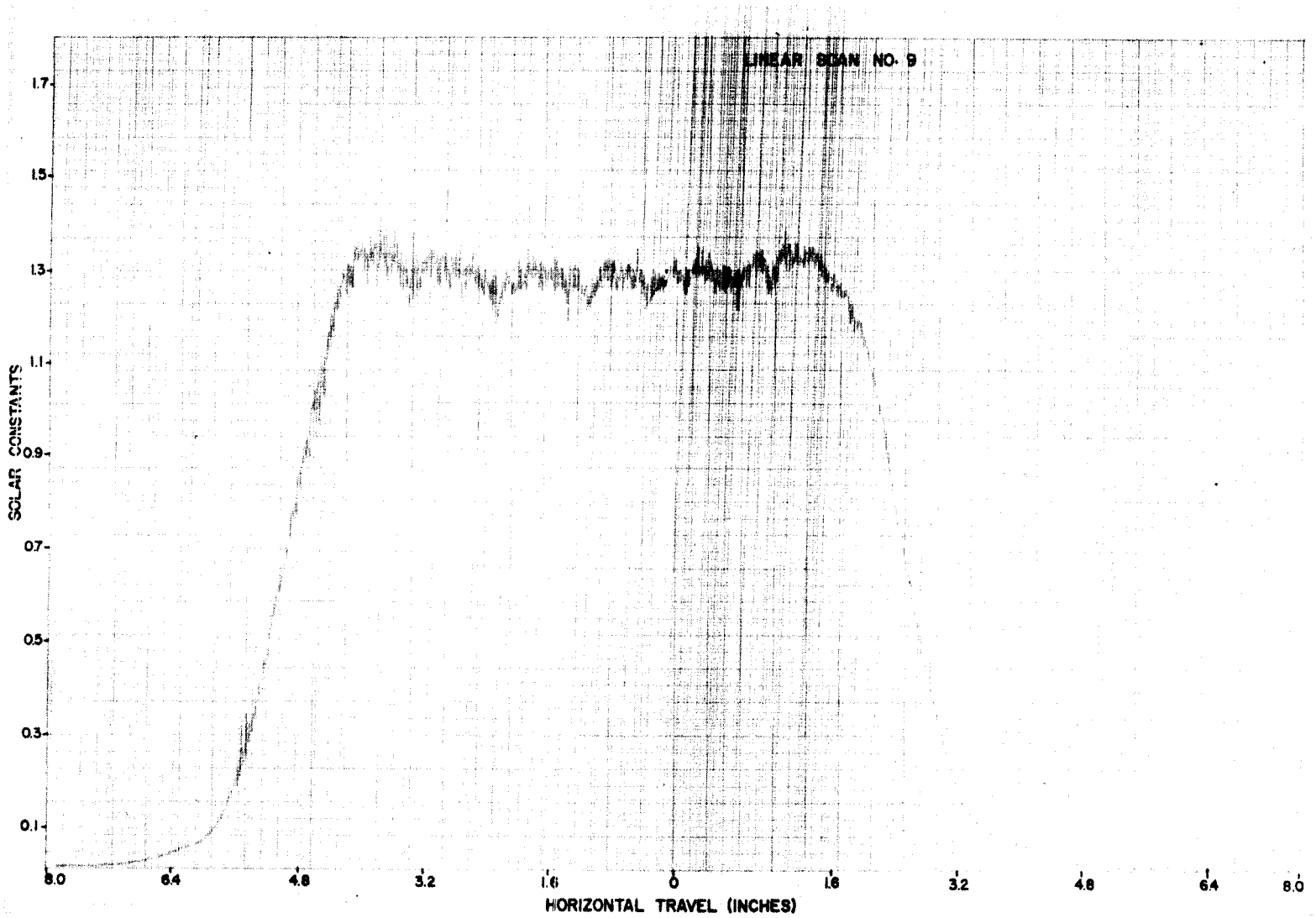

Figure 31–Linear Uniformity Scans

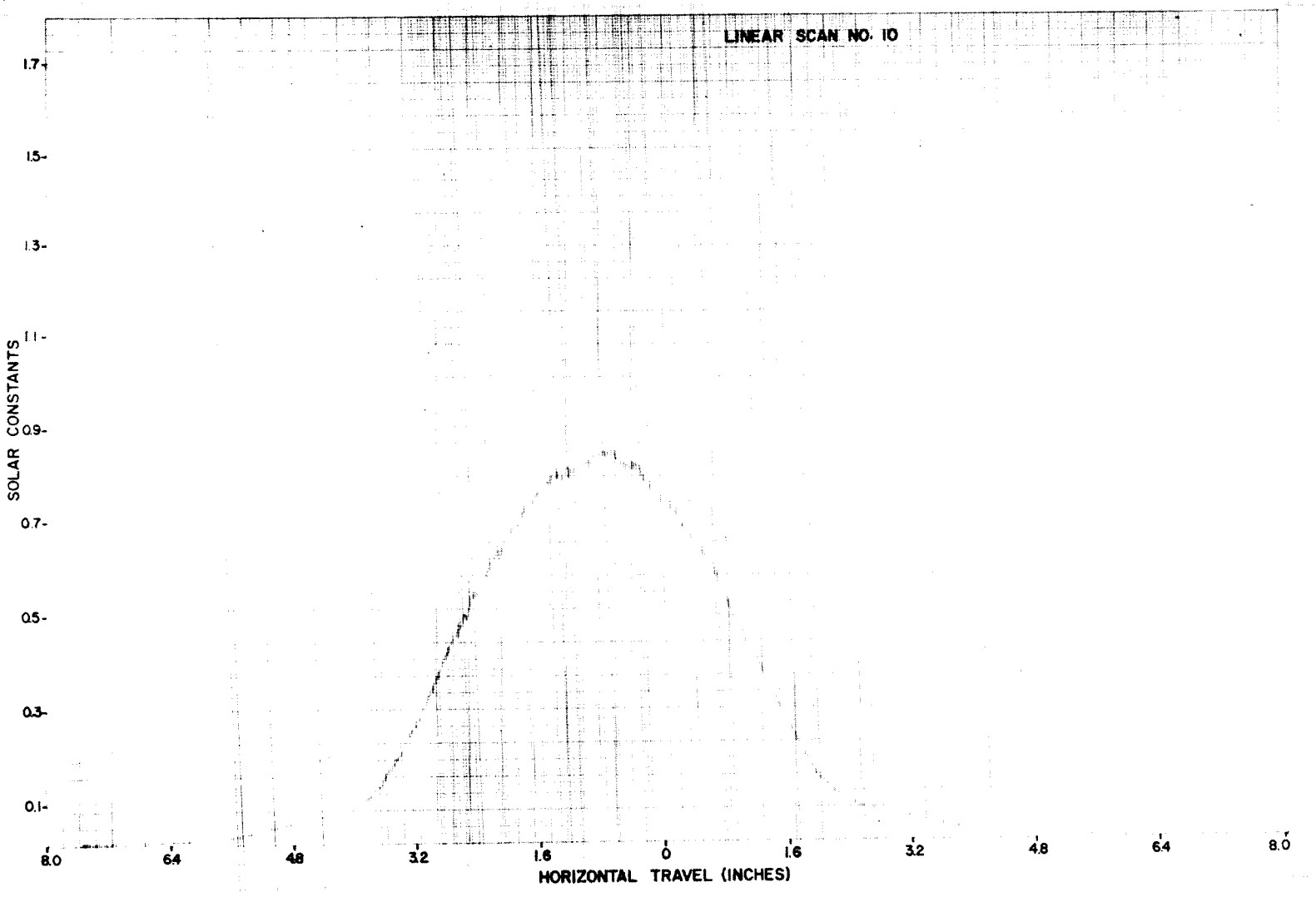

Figure 32–Linear Uniformity Scans

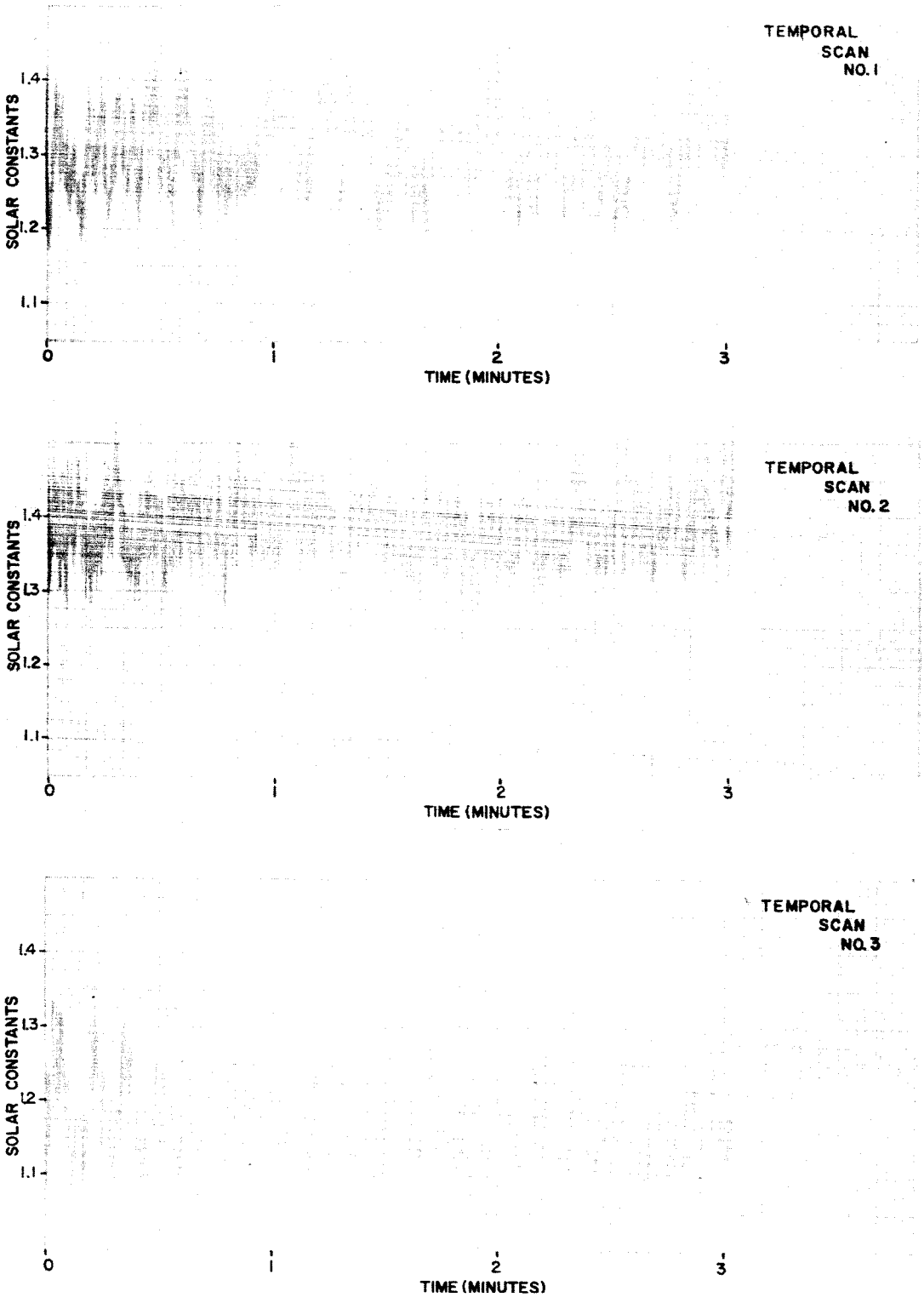

Figure 33–Temporal Uniformity Scans

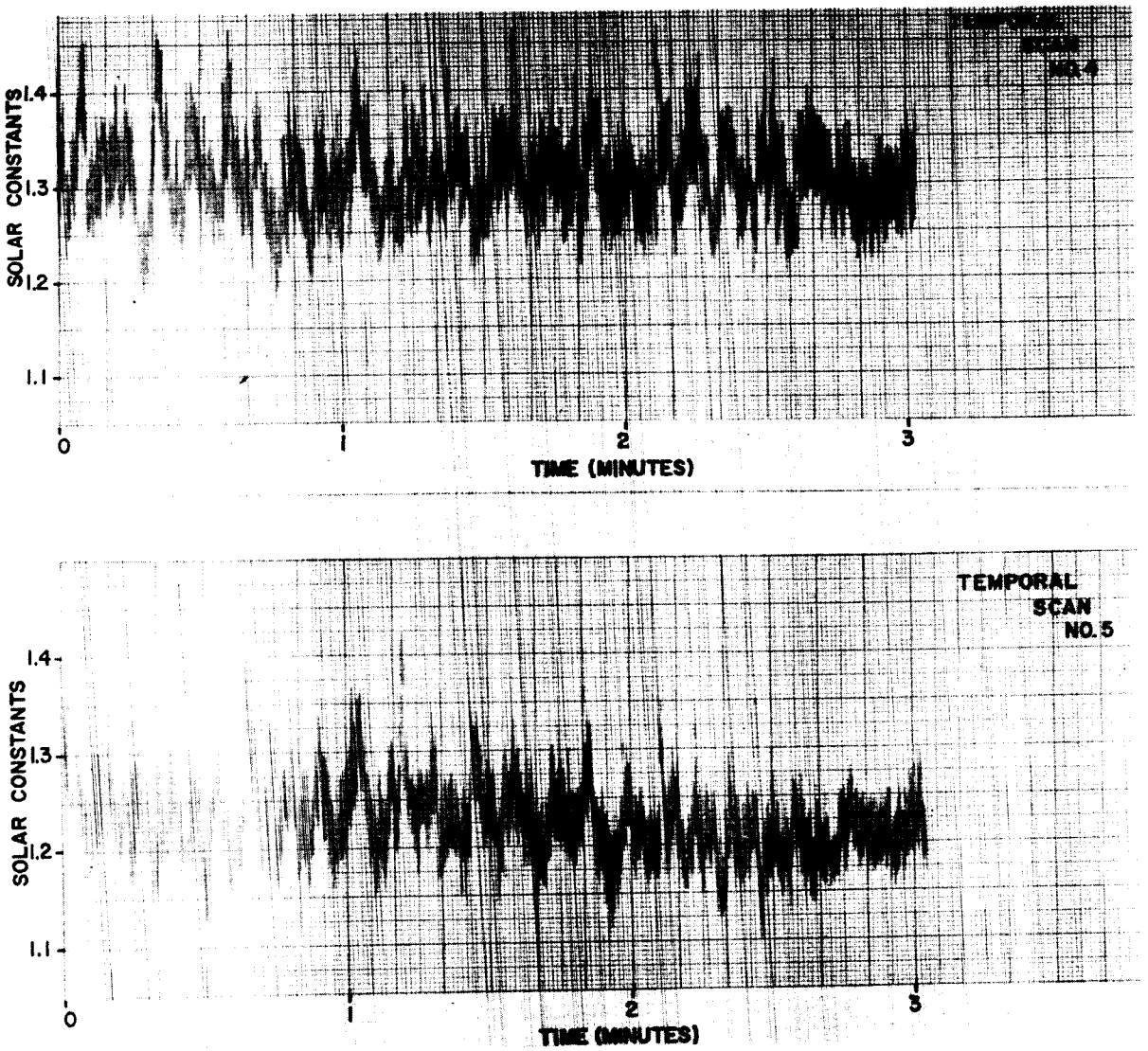

Figure 34–Temporal Uniformity Scans

			.58	.81	.52	.10			
		1.19	1.29	1.28	1.30	.89	.07		
	1.08	1.25	1.20	1.19	1.29	1.22	1.12	.19	
	1.26	1.30	1.26	1.23	1.22	1.24	1.32	.86	
.89	1.39	1.28	1.23	1.19	1.20	1.26	1.39	1.20	.27
1.01	1.55	1.39	1.31	1.27	1.30	1.36	1.46	1.33	.18
	1.49	1.33	1.25	1.23	1.25	1.31	1.17	.92	
	1.44	1.35	1.25	1.24	1.35	1.31	1.53	.65	
.20	.90	1.45	1.38	1.32	1.36	1.38	1.04	.20	.10
.02	.22	.95	1.51	1.49	1.51	1.13	.38	.20	.10

Figure 35–Beam Uniformity

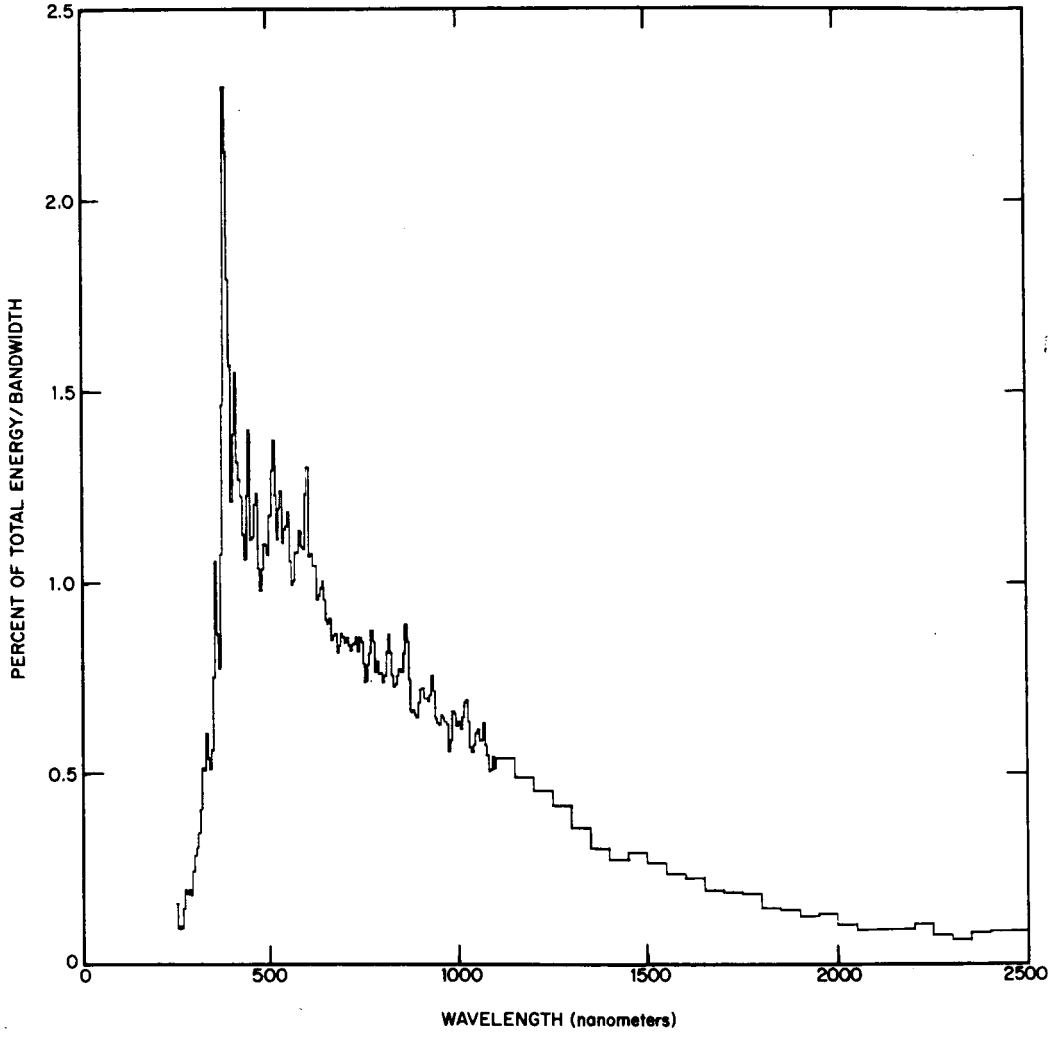

Figure 36–Carbon Arc (Bare)

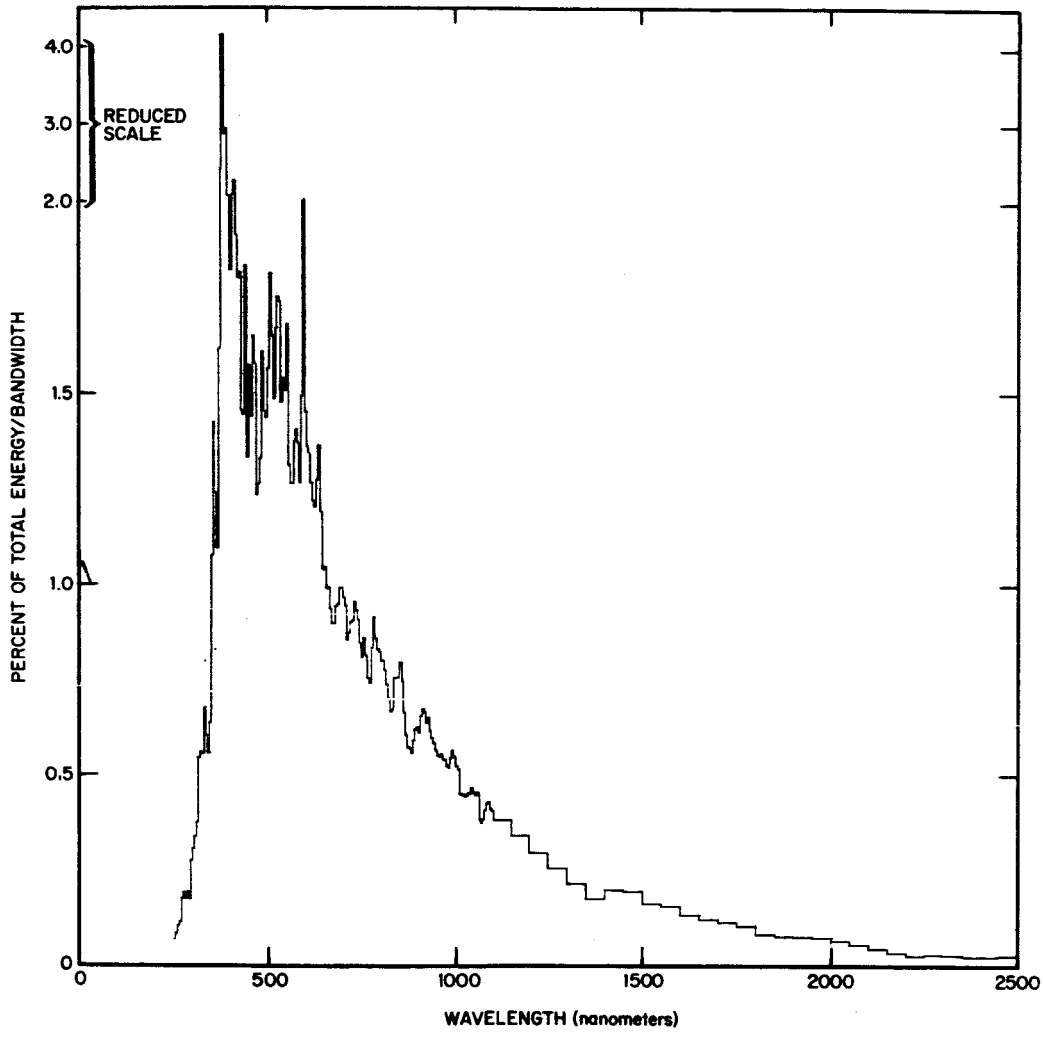

Figure 37–Carbon Arc (with Optical System)

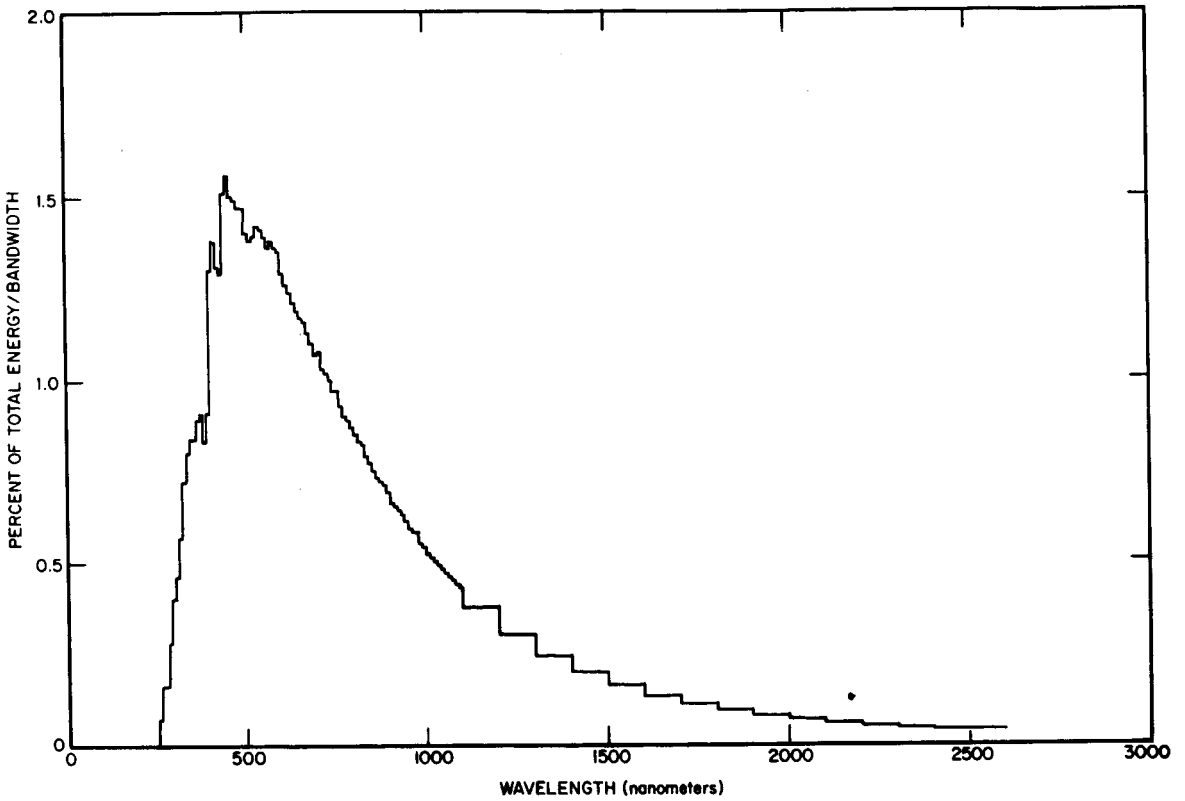

Figure 38–Johnson's Solar Measurements at Air Mass Zero
Given in Percent Energy Per 100 A Bandwidth

energy over A.M.O. solar at 380-400 nm, a deficiency from 400 nm to 800 nm, and an excess from 1000 nm to 2600 nm. When the quartz lens is introduced into the system these differences seem to be decreased. This is due not only to the filtering effect of the lens but also to the fact that the tail flame is contributing more illumination than in the former (bare arc) curve. The data was processed by computer using a Lagrangian interpolation for calculation of standard lamp values vs. wavelength.

The relative spectral distribution was then calculated and integrated over 5 or 50 nm intervals. The (area) under the curve between 250 nm and 2600 nm was set equal to 100%. In this manner curves can be compared as to relative spectral content. A printout of the computer data for the bare arc is shown in Table 3. Some absorptivities of materials are included in the printout.

ACKNOWLEDGMENT

I would like to give grateful acknowledgment of the assistance rendered by all members of the Radiometry Group.

TOTAL ABSORPTIVITY OF GOLD
17.724
TOTAL ABSORPTIVITY OF SILVER
4.040
TOTAL ABSORPTIVITY OF ALUMINUM
7.098
TOTAL ABSORPTIVITY OF TITANIUM OXIDE WITH SILICATE
22.174
TOTAL ABSORPTIVITY OF ZINC OXIDE WITH SILICONE
22.610
TOTAL ABSORPTIVITY OF TITANIUM OXIDE WITH SILICONE
19.761
TOTAL ABSORPTIVITY OF ZINC OXIDE WITH SILICATE
26.323
TOTAL ABSORPTIVITY OF 3M VELVET BLACK PAINT
97.222
TOTAL ABSORPTIVITY OF CAT-A-LAC BLACK PAINT
94.774
TOTAL ABSORPTIVITY OF CAT-A-LAC WHITE PAINT 12 COATS
19.577
TOTAL ABSORPTIVITY OF LEAFING ALUMINUM PAINT
27.799
TOTAL ABSORPTIVITY OF EVAP ALUM CRYOXIDE CLEANED 300 HRS UV
11.365
TOTAL ABSORPTIVITY OF IMP D BOTTOM SHELF ETU MODEL
16.241
TOTAL ABSORPTIVITY OF ACLAR COATED WITH IR81-E
20.547
TOTAL TRANSMISSION OF ACLAR COATED WITH IR81-E
46.825

WAVELENGTH	TEST LAMP ENERGY PER 10NM WAVELENGTH INTERVAL	SOLAR ENERGY	RATIO TEST LAMP/SOLAR
253.	0.159	0.071	2.25
258.	0.095	0.116	0.82
263.	0.099	0.162	0.61
268.	0.092	0.160	0.58
273.	0.145	0.162	0.89
278.	0.196	0.212	0.92
283.	0.183	0.283	0.65
288.	0.195	0.370	0.53
293.	0.180	0.445	0.41
298.	0.246	0.458	0.54
303.	0.286	0.465	0.62
308.	0.306	0.512	0.60
313.	0.345	0.576	0.60
318.	0.503	0.654	0.77
323.	0.515	0.728	0.71
328.	0.510	0.775	0.66
333.	0.605	0.809	0.75
338.	0.541	0.834	0.65
343.	0.511	0.849	0.60
348.	0.561	0.848	0.66

353.	0.752	0.849	0.89
358.	1.054	0.873	1.21
363.	0.862	0.900	0.96
368.	0.786	0.918	0.86
373.	1.072	0.920	1.17
378.	1.465	0.876	1.67
383.	2.298	0.839	2.74
388.	2.129	0.850	2.51
393.	1.793	0.920	1.95
398.	1.567	1.117	1.40
403.	1.214	1.314	0.92
408.	1.389	1.383	1.00
413.	1.550	1.395	1.11
418.	1.318	1.366	0.97
423.	1.270	1.324	0.96
428.	1.227	1.296	0.95
433.	1.125	1.304	0.86
438.	1.060	1.411	0.75
443.	1.228	1.526	0.80
448.	1.040	1.566	0.66
453.	1.113	1.577	0.71
458.	1.119	1.576	0.71
463.	1.203	1.567	0.77
468.	1.350	1.565	0.86
473.	1.138	1.557	0.73
478.	0.980	1.521	0.64
483.	1.036	1.486	0.70
488.	1.100	1.486	0.74
493.	1.099	1.486	0.74
498.	1.074	1.452	0.74
503.	1.176	1.415	0.83
508.	1.295	1.400	0.92
513.	1.372	1.395	0.98
518.	1.229	1.397	0.88
523.	1.112	1.405	0.79
528.	1.194	1.421	0.84
533.	1.241	1.435	0.86
538.	1.103	1.433	0.77
543.	1.141	1.425	0.80
548.	1.142	1.416	0.81
553.	1.184	1.405	0.84
558.	1.059	1.387	0.76
563.	0.996	1.375	0.72
568.	1.005	1.384	0.73
573.	1.080	1.395	0.77
578.	1.078	1.387	0.78
583.	1.133	1.375	0.82
588.	1.097	1.372	0.80
593.	1.087	1.365	0.80
598.	1.234	1.335	0.92
603.	1.300	1.304	1.00
608.	1.069	1.286	0.83
613.	1.077	1.274	0.85
618.	1.043	1.263	0.83
623.	1.043	1.253	0.83
628.	0.958	1.238	0.77
633.	0.969	1.223	0.79
638.	0.983	1.212	0.81
643.	1.005	1.203	0.84
648.	0.956	1.192	0.80

653.	0.901	1.183	0.76
658.	0.893	1.178	0.76
663.	0.906	1.172	0.77
668.	0.849	1.159	0.73
673.	0.861	1.142	0.75
678.	0.866	1.127	0.77
683.	0.817	1.112	0.74
688.	0.834	1.094	0.76
693.	0.866	1.082	0.80
698.	0.858	1.088	0.79
703.	0.845	1.092	0.77
708.	0.856	1.068	0.80
713.	0.835	1.041	0.80
718.	0.821	1.034	0.79
723.	0.839	1.031	0.81
728.	0.839	1.022	0.82
733.	0.857	1.011	0.85
738.	0.819	0.994	0.82
743.	0.856	0.980	0.87
748.	0.842	0.981	0.86
753.	0.788	0.980	0.80
758.	0.739	0.962	0.77
763.	0.782	0.940	0.83
768.	0.817	0.923	0.88
773.	0.877	0.910	0.96
778.	0.845	0.904	0.93
783.	0.767	0.900	0.85
788.	0.795	0.890	0.89
793.	0.760	0.879	0.86
798.	0.761	0.869	0.88
803.	0.739	0.859	0.86
808.	0.754	0.848	0.89
813.	0.817	0.839	0.97
818.	0.862	0.835	1.03
823.	0.817	0.829	0.99
828.	0.757	0.814	0.93
833.	0.727	0.798	0.91
838.	0.731	0.788	0.93
843.	0.754	0.778	0.97
848.	0.770	0.768	1.00
853.	0.766	0.758	1.01
858.	0.811	0.747	1.09
863.	0.890	0.738	1.21
868.	0.846	0.732	1.16
873.	0.743	0.728	1.02
878.	0.659	0.723	0.91
883.	0.666	0.718	0.93
888.	0.655	0.709	0.92
893.	0.648	0.697	0.93
898.	0.682	0.682	1.00
903.	0.719	0.667	1.08
908.	0.721	0.661	1.09
913.	0.697	0.657	1.06
918.	0.697	0.652	1.07
923.	0.689	0.647	1.07
928.	0.702	0.642	1.09
933.	0.754	0.637	1.18
938.	0.716	0.627	1.14
943.	0.644	0.617	1.04
948.	0.631	0.606	1.04

953.	0.628	0.596	1.05
958.	0.651	0.590	1.10
963.	0.644	0.586	1.10
968.	0.634	0.588	1.08
973.	0.629	0.586	1.07
978.	0.557	0.572	0.98
983.	0.587	0.556	1.06
988.	0.661	0.550	1.20
993.	0.657	0.546	1.20
998.	0.628	0.536	1.17
1003.	0.632	0.526	1.20
1008.	0.617	0.520	1.19
1013.	0.648	0.515	1.26
1018.	0.684	0.510	1.34
1023.	0.690	0.505	1.37
1028.	0.635	0.500	1.27
1033.	0.569	0.495	1.15
1038.	0.558	0.490	1.14
1043.	0.575	0.485	1.19
1048.	0.606	0.480	1.26
1053.	0.615	0.475	1.29
1058.	0.587	0.470	1.25
1063.	0.587	0.465	1.26
1068.	0.631	0.460	1.37
1073.	0.574	0.455	1.26
1078.	0.548	0.450	1.22
1083.	0.505	0.445	1.13
1088.	0.509	0.227	2.24
1093.	0.544	0.435	1.25
1098.	0.512	1.770	0.29
1125.	0.539	0.383	1.41
1175.	0.490	0.908	0.54
1225.	0.455	0.306	1.48
1275.	0.416	0.275	1.51
1325.	0.358	0.247	1.45
1375.	0.302	0.222	1.36
1425.	0.273	0.200	1.36
1475.	0.292	0.181	1.61
1525.	0.263	0.164	1.61
1575.	0.236	0.149	1.58
1625.	0.228	0.135	1.69
1675.	0.196	0.123	1.59
1725.	0.190	0.112	1.70
1775.	0.185	0.103	1.81
1825.	0.148	0.094	1.57
1875.	0.142	0.087	1.64
1925.	0.129	0.080	1.62
1975.	0.131	0.074	1.78
2025.	0.104	0.068	1.54
2075.	0.090	0.062	1.44
2125.	0.101	0.058	1.75
2175.	0.091	0.053	1.70
2225.	0.105	0.050	2.12
2275.	0.078	0.046	1.71
2325.	0.067	0.042	1.57
2375.	0.086	0.042	2.06
2425.	0.085	0.037	2.28